Carbon and Nitrogen Cycle Dynamic in Continental Late-Carboniferous to Early Permian Basins of Eastern Pangea (Northeastern Massif Central, France)

Mathilde Mercuzot[1]*, Christophe Thomazo[2,3], Johann Schnyder[4], Pierre Pellenard[2], François Baudin[4], Anne-Catherine Pierson-Wickmann[1], Pierre Sans-Jofre[5], Sylvie Bourquin[1], Laurent Beccaletto[6], Anne-Lise Santoni[2], Georges Gand[2], Matthieu Buisson[4,7], Laure Glé[2], Thomas Munier[2], Antonios Saloume[4], Mohamed Boussaid[4] and Tracy Boucher[4]

[1]Univ Rennes, CNRS, Géosciences Rennes - UMR 6118, Rennes, France, [2]Biogéosciences UMR uB/CNRS 6282, Université Bourgogne Franche-Comté, Dijon, France, [3]Institut Universitaire de France, Paris, France, [4]Institut des Sciences de la Terre de Paris (ISTeP), UMR 7193 CNRS, Sorbonne Université, Paris, France, [5]MNHN, CNRS UMR 7590, IRD, Institut de minéralogie, Physique des Matériaux et de Cosmochimie, Sorbonne Université, Paris, France, [6]BRGM, Orléans, France, [7]Université de Paris - Institut de physique du globe de Paris - CNRS, UMR 7154, Paris, France

Late Carboniferous to early Permian organic-rich sedimentary successions of late-orogenic continental basins from the northeastern Massif Central (France) coincide with both the Variscan mountain dismantling and the acme of the long-lasting Late Paleozoic Ice Age. Here, we investigate the carbon and nitrogen cycles in the newly dated sedimentary successions of the Decize–La Machine and Autun basins during these geodynamic and climate upheavals. The sedimentary organic matter has been analyzed through Rock-Eval pyrolysis, palynofacies and elemental and isotope geochemistry along cored-wells and outcropping sections, previously accurately defined in terms of paleo-depositional environments. Rock-Eval and palynofacies data have evidenced two origins of organic matter: a phytoplanktonic/bacterial lacustrine origin (Type I organic matter, organic $\delta^{13}C$ values around −23.5‰), and a terrestrial origin (vascular land plants, Type III organic matter, organic $\delta^{13}C$ values around −20‰), mixed in the deltaic-lacustrine sediments during background sedimentation (mean organic $\delta^{13}C$ values around −22‰). Episodes of high organic matter storage, reflected by black shales and coal-bearing deposits (total organic carbon up to 20 and 70%, respectively) are also recognized in the successions, and are characterized by large negative organic carbon isotope excursions down to −29‰. We suggest that these negative isotope excursions reflect secondary processes, such as organic matter remineralization and/or secondary productivity varying under strict local controls, or possibly larger scale climate controls. At times, these negative $\delta^{13}C$ excursions are paired with positive $\delta^{15}N$ excursions up to +10‰, reflecting water column denitrification and anammox during lake-water stratification episodes. Together, these isotopic signals (i.e., low sedimentary organic $\delta^{13}C$ associated with high bulk $\delta^{15}N$ values) indicate periods of high primary productivity of

surface waters, where nitrogen and carbon cycles are spatially decoupled. These local processes on the sedimentary isotope archives may partially blur our ability to directly reconstruct paleoclimate variations in such continental settings using only C and N isotopes. At last, we explore an organic δ^{13}C-based mixing model to propose ways to disentangle autochthonous versus allochthonous origin of organic matter in lacustrine continental settings.

INTRODUCTION

The late Carboniferous to early Permian period (~300 Ma) is largely recognized for its high primary productivity on lands, and witnesses the highest rates of global organic carbon burial of the Phanerozoic Eon preserved in the sedimentary rocks (e.g., Klemme and Ulmishek, 1991; Maynard et al., 1997; Berner, 2003; Schwarzbauer and Jovančićević, 2015; Montañez, 2016). Indeed, coal forests (wetland biome) occupied large areas within the intertropical zone during this time interval (Cleal and Thomas, 2005).

The continental sediments archived during this time window reflect different parameters including first-order tectonics, controlling the structure and subsidence history of sedimentary basins of the late Variscan orogenic setting, and paleoclimate. During the Carboniferous–Permian transition (CPT), the latter is characterized by the acme of the Late Paleozoic Ice Age (LPIA, late Devonian to late Permian, Isbell et al., 2003; Fielding et al., 2008; Isbell et al., 2012; Montañez and Poulsen, 2013; Soreghan et al., 2019), associated with humid belts promoting organic-matter (OM) production in the intertropical zone (e.g., Scotese, 2016) and followed by global warming and aridification until the early Triassic. The onset and duration of the LPIA resulted from several parameters such as paleogeographic and geodynamic changes (landmass merging towards southern high latitudes, erection of reliefs at the equator, Powell and Veevers 1987; Veevers, 1994; Opdyke et al., 2001; Frank et al., 2008; Isbell et al., 2012; Domeier and Torsvik, 2014), an increase in chemical weathering of Variscan reliefs (Goddéris et al., 2017), astronomical forcing (e.g., low incident solar luminosity, albedo feedbacks, Crowley and Baum, 1992; Hyde et al., 1999), and an enhanced volcanic activity (sulfate aerosols, Soreghan et al., 2019). Thus, relief erosion and alteration products triggered high sedimentary fluxes, which are recorded in the CPT basins.

The late Carboniferous to early Permian period exhibits substantial variations in the global carbon cycle, with the highest ^{13}C enrichment in carbonates of the Phanerozoic, with carbonate δ^{13}C values as high as 5‰ (Strauss and Peters-Kottig, 2003). This isotope excursion is usually interpreted as reflecting a carbon cycle dominated by a very high burial rate of OM in the sediments, in agreement with OM-rich deposit evidences (Berner and Raiswell, 1983; Beauchamp et al., 1987; Berner, 1989; Bruckschen et al., 1999; Hayes et al.,

1999; Mii et al., 1999; Mii et al., 2001; Saltzman et al., 2004; Saltzman, 2005; Peters-Kottig et al., 2006; Frank et al., 2008, Grossman et al., 2008; Liu et al., 2017; Liu et al., 2018).
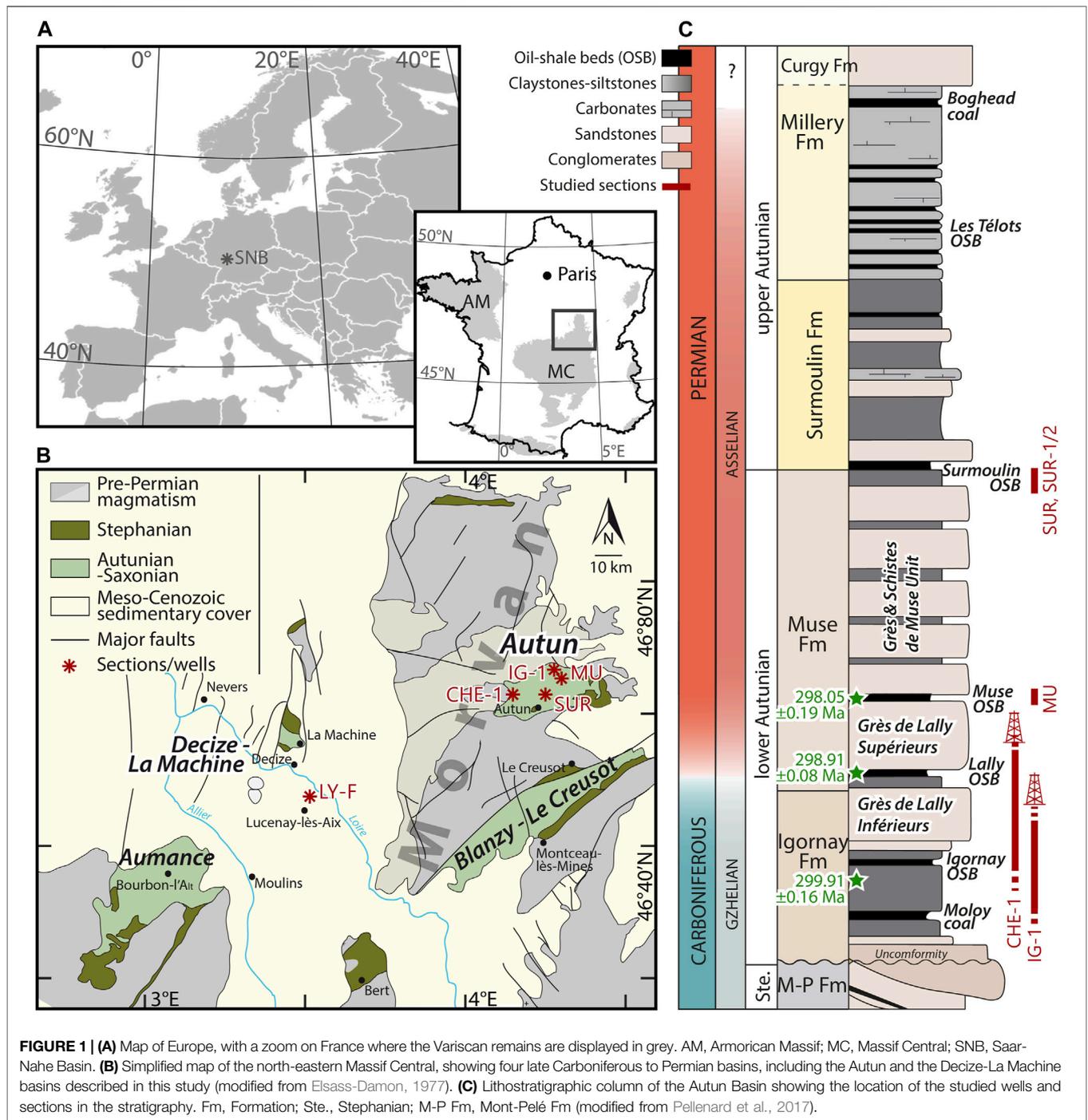
While sedimentological context of northeastern Massif Central CPT basins (France) has been recently updated (Ducassou et al., 2019; Mercuzot et al., 2021; Mercuzot et al., submitted), both the dynamics of OM production and preservation are poorly documented in these areas, except for a few studies (Elsass-Damon 1977; Garel et al., 2017). Moreover, the OM isotopic characterization is still lacking in most studies on continental series from this period, although many studies have successfully demonstrated that carbon and nitrogen isotope signals of OM help to decipher its production (primary productivity), preservation (remineralization), and paleoclimate dynamics (e.g., Hollander and McKenzie, 1991; Hollander et al., 1993; Altabet and Francois, 1994; Schubert and Calvert, 2001; Sephton et al., 2002; Deutsch et al., 2004; Algeo et al., 2008; Kashiyama et al., 2008; Ramaswamy et al., 2008; Schnyder et al., 2009; Thomazo et al., 2009; Jenkyns, 2010; Ader et al., 2014; Ader et al., 2016; Wang et al., 2017).

In this study, we aim to describe the sedimentary dynamics of OM and associated geochemical signatures from recently radio-isotopically-dated continental series of the northeastern Massif Central (Pellenard et al., 2017; Ducassou et al., 2019).

Using elemental and isotope (δ^{13}C and δ^{15}N) geochemistry through Rock Eval pyrolysis and Isotope Ratio Mass Spectrometry (IRMS), paired with OM characterization through palynofacies analyses, we discuss the origin and preservation of archived OM in the CPT northeastern Massif Central basins, and describe the processes associated with the biogeochemical cycling of carbon and nitrogen through time and space in deep-time lacustrine-dominated environments. Local, facies-related controls on the OM sedimentation relative to global signals are also considered in the light of known trends in the carbon and nitrogen global cycle across the LPIA period.

GENERAL GEOLOGICAL SETTING

The late Variscan orogenic evolution of Western Europe is characterized by two syn-to late- extensional tectonic events (i.e. D4 and D5 events from Faure et al., 2009): 1) a mid-Carboniferous syn-orogenic ductile extensional event, synchronous with pluton emplacement, widespread crustal-derived plutonism and volcanism, and local development of volcano-sedimentary basins, and 2) a late Carboniferous-early

FIGURE 1 | (A) Map of Europe, with a zoom on France where the Variscan remains are displayed in grey. AM, Armorican Massif; MC, Massif Central; SNB, Saar-Nahe Basin. **(B)** Simplified map of the north-eastern Massif Central, showing four late Carboniferous to Permian basins, including the Autun and the Decize-La Machine basins described in this study (modified from Elsass-Damon, 1977). **(C)** Lithostratigraphic column of the Autun Basin showing the location of the studied wells and sections in the stratigraphy. Fm, Formation; Ste., Stephanian; M-P Fm, Mont-Pelé Fm (modified from Pellenard et al., 2017).

Permian late-orogenic extension, characterized by the uplift of high-grade metamorphic domes and related faults and detachments, and the development of mainly half-graben basins, like the Autun Basin. These two events were triggered by the collapse of the Variscan mountain belt (Ménard and Molnar, 1988; Valle et al., 1988; Van Den Driessche and Brun, 1989; Burg et al., 1990; Malavieille et al., 1990; Van Den Driessche and Brun, 1992; Faure and Becq-Giraudon 1993; Burg et al., 1994; Faure 1995; Becq-Giraudon et al., 1996; Choulet et al., 2012). This

WE-oriented mountain belt was located in equatorial position and has influenced the late Paleozoic global climate dynamics (e.g., Goddéris et al., 2017) reflected by the LPIA, constituting a major glaciation on a vegetated Earth (Gastaldo et al., 1996; Montañez et al., 2007). The paroxysmal phase of the LPIA occurred at the end of the Carboniferous and during the earliest Permian (ca. 305–290 Ma, Isbell et al., 2003; Fielding et al., 2008; Isbell et al., 2012; Montañez and Poulsen, 2013; Soreghan et al., 2019), a period that records both extremely low CO_2 levels (roughly equivalent to

present-day levels, between 100 and 1,000 ppm, Berner, 2001; Montañez et al., 2007; Foster et al., 2017) and the highest O_2 levels (nearly twice the present-day atmospheric level) in probably the entire Earth history (Berner and Canfield, 1989).

The Decize–La Machine and Autun basins, located in the northeastern French Massif Central (**Figures 1A,B**) record the collapse of the Variscan mountain through their late CPT sedimentary successions (Pellenard et al., 2017; Ducassou et al., 2019). These basins have recently been re-investigated to improve their sedimentological and chronological settings (Garel et al., 2017; Pellenard et al., 2017; Ducassou et al., 2019; Mercuzot et al., 2021; Mercuzot et al., submitted), but their biogeochemical characteristics remain poorly documented to date.

Recently, Mercuzot et al. (2021) have proposed that the Decize–La Machine and Autun basins may have been connected at the time of their filling, and that they probably reflect paleo-depocenters of a larger sedimentary basin, encompassing other nearby basins, notably the southward Blanzy–Le Creusot Basin and the eastward Aumance Basin (**Figure 1B**), and possibly the Carboniferous–Permian series beneath the Meso-Cenozoic sedimentary cover of the Paris Basin (Contres, Brécy and Arpheuilles basins, Beccaletto et al., 2015; Mercuzot et al., 2021; Mercuzot et al., submitted). Consequently, the sedimentary successions of the Decize–La Machine and Autun basins could be part of a much larger sedimentary area than previously considered and could have archived and participated in the secular evolution of the global carbon cycle at that time. It is therefore interesting to investigate the organic geochemical signals recorded in these areas.

The Decize–La Machine Basin is partly outcropping (La Machine area), and partly located beneath the Meso-Cenozoic sedimentary cover of the Paris Basin (Lucenay-lès-Aix area, **Figure 1B**). Our work is based on the study of the reference LY-F cored-well (**Figure 1B**), whose sediments were deposited between 299 ± 2 and 294 ± 2/−7 Ma—ages obtained by LA-ICP-MS dating (Laser Ablation–Induced Coupled Plasma–Mass Spectrometry) on zircon and apatite by Ducassou et al. (2019).

In the Autun Basin, five sections are investigated, respectively the IG-1, CHE-1, MU, SUR-1, SUR-2 cored-wells and the SUR outcrop (**Figure 1C**). The base of the IG-1 core has been dated at 299.91 ± 0.16 Ma and the top of the Muse outcrop (approximatively corresponding to the top of the MU core) at 298.05 ± 0.19 Ma, using the U-Pb CA-ID-TIMS method (Chemical Abrasion–Isotopic Dilution–Thermal Ionization Mass Spectrometry, Pellenard et al., 2017).

DEPOSITIONAL ENVIRONMENTS IN THE NORTHEASTERN MASSIF CENTRAL BASINS

The Lucenay-lès-Aix area presents a variety of continental depositional environments, ranging from coastal plain, with coal-bearing levels formed in swamps, to lake, with occurrences of deltaic systems that evolve to deep lake deposits toward the east, according to the observations of sedimentological facies and seismic profiles in this part of the
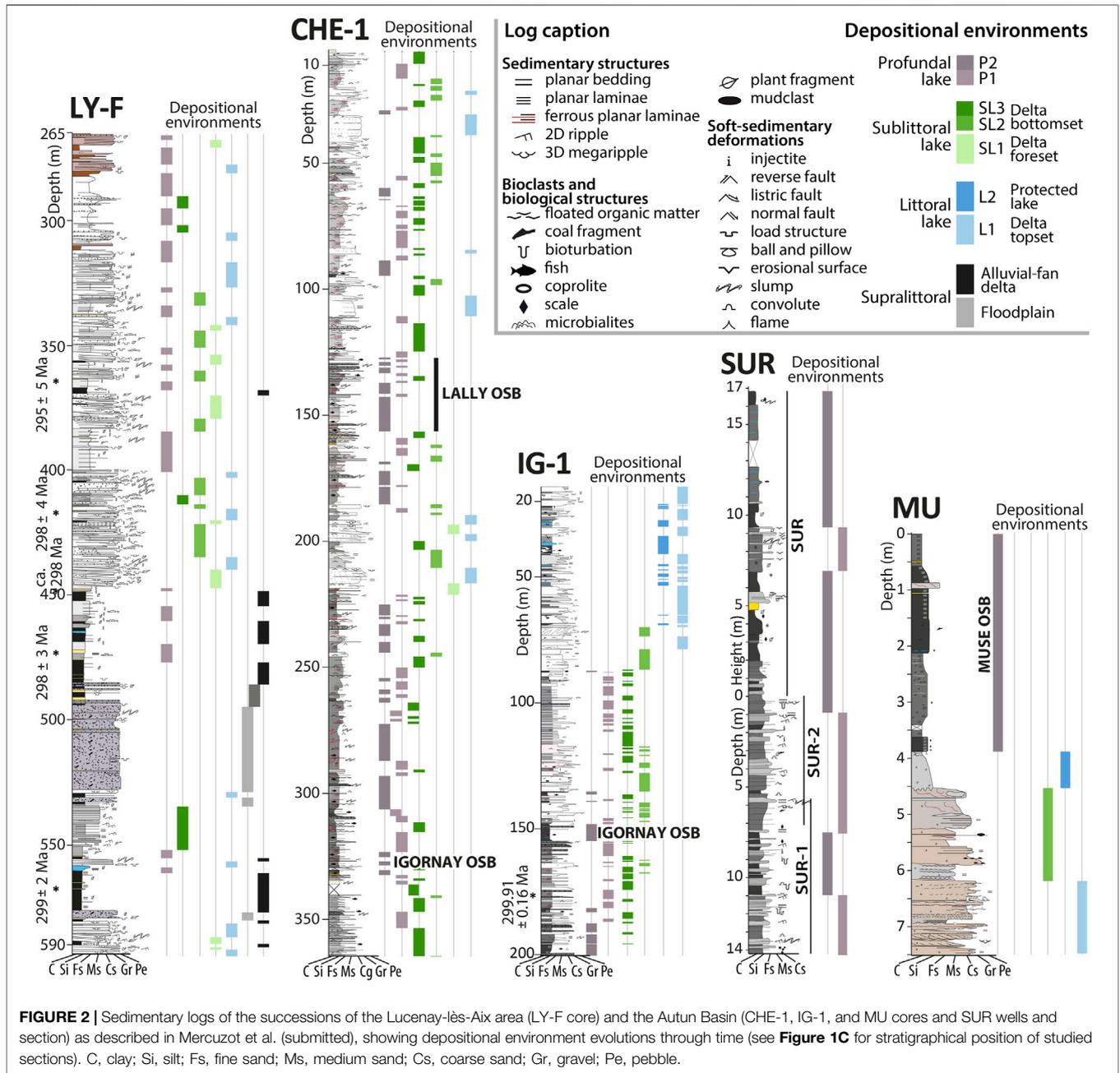
basin (Ducassou et al., 2019; Mercuzot et al., 2021). The general depositional context is typical of differentiated Gilbert-type deltas, with inclined foreset and bottomset features (mostly coarse-grained), sinking into a lake environment characterized by fine-grained deposits (**Figure 2**). This lacustrine environment is located either at the end of the deltaic complexes or laterally to the sediment input. In the second case, microbial deposits may be found, indicating a water depth within the photic zone.

The sedimentological setting of the Autun Basin was firstly investigated by Marteau (1983), and recently by Mercuzot et al. (submitted). The sedimentary succession shows mainly lacustrine facies with occurrences of deltaic facies and OM-rich levels corresponding to black shales, namely oil-shale beds, OSBs (**Figure 2**). The base of the Autun Basin sedimentary succession is characterized by deep lacustrine deposits, showing well-developed OSBs alternating with episodic distal turbidites, and the sediment supply is provided to the basin by deltaic distributaries (Mercuzot et al., submitted). Three main depositional environments have been defined, based on the classification of Bohacs et al. (2000) (**Figure 2**): the profundal, the sublittoral and the littoral lake environments, from the more distal to the more proximal, the two latter encompassing deltaic deposits. Due to the dominance of sublittoral to profundal lacustrine facies in this area (Mercuzot et al., submitted), and the consistence with the chronostratigraphic framework, it has been suggested that the Autun Basin could be the distal equivalent of the Lucenay-lès-Aix area proximal series, with major sedimentary supplies coming from the west (Mercuzot et al., 2021).

In both areas, where sediment supply is minimal, OM-rich deposits are observed as coal accumulations in the Lucenay-lès-Aix area and OSBs in the Autun Basin (**Figure 2**). The coal levels were formed in a supralittoral environment (floodplain), mainly by accumulation of vascular land plant remains, whereas OSBs were deposited in a profundal lake environment, mainly fed by primary productivity in the water column (phytoplankton) with additional terrestrial OM (Garel et al., 2017).

MATERIAL AND METHODS

Geochemical analyses were carried out on samples collected in both areas, from cored-well and outcrop sections. The sections are from the Lucenay-lès-Aix area (LY-F well, 329 m) and from the Autun Basin (IG-1 well, 200 m; CHE-1 well, 365 m; MU well, 7.5 m; SUR 1 and 2 wells, 14 m in total; SUR outcrop, 17 m). The SUR-1 and SUR-2 cores were acquired for this study at the base of the SUR outcrop. The cores were drilled vertically, using a modified portable Shawtool Drill machine (diamond bit, 41 mm diameter) lubricated by fresh water from an adjacent river. It is important to note that the MU and SUR sections represent sedimentary intervals of very short duration compared to the 3 other wells. Each section was sampled every 1–2 m in fine-grained lithologies (sometimes with significantly higher resolution such as for the MU core and the Igornay OSBs of the IG-1 core, i.e., each 10 cm). The samples were then ground with a ring and puck mill at the Biogéosciences

FIGURE 2 | Sedimentary logs of the successions of the Lucenay-lès-Aix area (LY-F core) and the Autun Basin (CHE-1, IG-1, and MU cores and SUR wells and section) as described in Mercuzot et al. (submitted), showing depositional environment evolutions through time (see **Figure 1C** for stratigraphical position of studied sections). C, clay; Si, silt; Fs, fine sand; Ms, medium sand; Cs, coarse sand; Gr, gravel; Pe, pebble.

laboratory (Université Bourgogne–Franche-Comté, France) in order to obtain a 60-μm sample powder.

Rock-Eval Pyrolysis

Samples from IG-1 (215 samples), CHE-1 (329 samples), MU (34 samples), SUR (42 samples) and SUR 1 and 2 (8 samples) sections were analyzed using a Rock-Eval 6 Turbo apparatus (Vinci Technologies) at the ISTeP laboratory (Sorbonne Université) following the method described by Behar et al. (2001). These measurements were obtained from the successive pyrolysis and oxidation of ~60 μg of powder. The amount of free hydrocarbons is given by the S1 signal, while the S2 signal corresponds to the

hydrocarbons generated from the cracking of the kerogen between 300 and 650°C. The temperature at which the maximum hydrocarbon yield occurs (Tmax) is used to monitor the OM thermal maturation. The quantity of CO_2 and CO generated during pyrolysis and oxidation is continuously detected and related to organic and inorganic carbon contents, depending on decomposition temperature. The total organic carbon (TOC, wt.%) is calculated as the sum of pyrolzsed and oxidized organic carbon. Hydrogen (HI) and oxygen (OI) indexes are expressed in mgHC/gTOC (HC: hydrocarbon) and mgCO$_2$/gTOC, respectively, and result from the S2/TOC × 100 and from the S3/TOC × 100 calculations.

Palynofacies Characterization

Palynofacies aim to study the organic constituents of a sediment under optical microscope (Combaz, 1964; Tyson, 1995), in order to assess their origin(s) and preservation state (Batten, 1982; McArthur et al., 2016; Schnyder et al., 2017). In order to remove carbonates and silicates, bulk-rock samples were treated by HCl-HF using standard method developed by Steffen and Gorin (1993). The organic residues were then used to make total, non-filtered and filtered slides (the latter using a 10-μm sieve mesh). Palynofacies observations were performed using an Axioplan2 Imaging Zeiss microscope in transmitted light at the ISTeP laboratory. Five samples were selected from the IG-1 core, six samples from the MU core and ten samples from the CHE-1 core, in order to obtain a general and qualitative assessment of the particulate OM. The samples were selected to document the range of varying TOC and HI values obtained through Rock-Eval pyrolysis.

Elemental and Isotope Analyses

Organic carbon and bulk nitrogen isotopic compositions were analyzed on the LY-F (98 samples), IG-1 (222 samples), CHE-1 (98 samples), MU (32 samples) and SUR, SUR-1 and SUR-2 (21 samples) sections. For IG-1, CHE-1, MU, and SUR samples, containing some carbonates such as calcite, dolomite and siderite, carbonate-free residues were produced by mixing sample powders with 6N HCl during 24 h. The powder was then rinsed with deionized distilled water to a neutral pH and oven-dried at 50°C for 12 h. The total carbonate content, expressed in weight percent (wt.%), was evaluated by gravimetric quantification. The residues were then poured into tin capsules (2–200 mg) using a Sartorius M2P ultra-balance before isotope measurements were performed using a Vario MICRO cube (Elementar GmbH, Hanau, Germany) elemental analyser, coupled to an Isoprime (Elementar, Manchester, United Kingdom) isotope ratio mass spectrometer (EA-IRMS) at the Biogéosciences laboratory. Certified USGS40 ($\delta^{13}C_{org}$ = −26.2‰, C_{org} = 40.82 wt.% and $\delta^{15}N$ = −4.5‰, N = 9.52 wt.%) and caffeine IAEA-600 ($\delta^{13}C_{org}$ = −27.77‰, and $\delta^{15}N$ = 1‰) reference materials were used for the calibration. Isotope results are reported in delta-notation relative to V-PDB and to AIR for carbon and nitrogen isotopes, respectively. Replicates were made for each sample except for the LY-F sample set. The external reproducibility (1σ), based on sample replicate analyses, is better than ±0.06‰ for the $\delta^{13}C_{org}$ and ±0.17‰ for the $\delta^{15}N_{bulk}$. Total organic carbon (TOC) and total nitrogen (organic and mineral nitrogen, TN) contents are expressed in dry weight percentage (wt.%) of the bulk powder, and have a mean 1 σ reproducibility of ±0.11 wt.% and ±0.18 wt.%, respectively.

For LY-F samples, carbonate-free residues were produced by mixing sample powder with 2N HCl in an ultrasonic bath before rinsing and drying at 60°C. The $\delta^{13}C_{org}$ values were determined using an elemental analyser (VarioCube) interfaced with an isotope ratio mass spectrometer (VG Isoprime), at the Stable Isotope Laboratory of the PEGASE Joint Research Unit (INRAE, Saint-Gilles, France). International standards USGS 24 (with $\delta^{13}C$ = −16.5 ± 0.1‰, n = 36) and ANU sucrose (with $\delta^{13}C$ = −10.5 ± 0.1‰, n = 35) were used as reference materials. The reproducibility of $\delta^{13}C$ values is better than ±0.2‰, based on repeated measurements of samples and standards.

RESULTS

Rock-Eval Pyrolysis

All the following mean values for the analysis panel are given associated with their standard deviation (±1σ).

In the IG-1 core, Tmax values range from 369 to 520°C with a mean value of 437 ± 12°C, TOC values range from 0.12 to 20.36 wt.% with a mean value of 4.76 ± 4.58 wt.% (**Figure 3**), HI values range from 28 to 587 mgHC/gTOC with a mean value of 231 ± 151 mgHC/gTOC and OI values range between 0 and 131 mgCO₂/gTOC with a mean value of 14 ± 18 mgCO₂/gTOC (**Supplementary Table 1**). The TOC curve displays five intervals of very high values (>5 wt.%, **Figure 3**), between ~200 and 180 m, ~160 and 130 m, ~90 and 70 m–35 and 45 m, and at ~22 m.

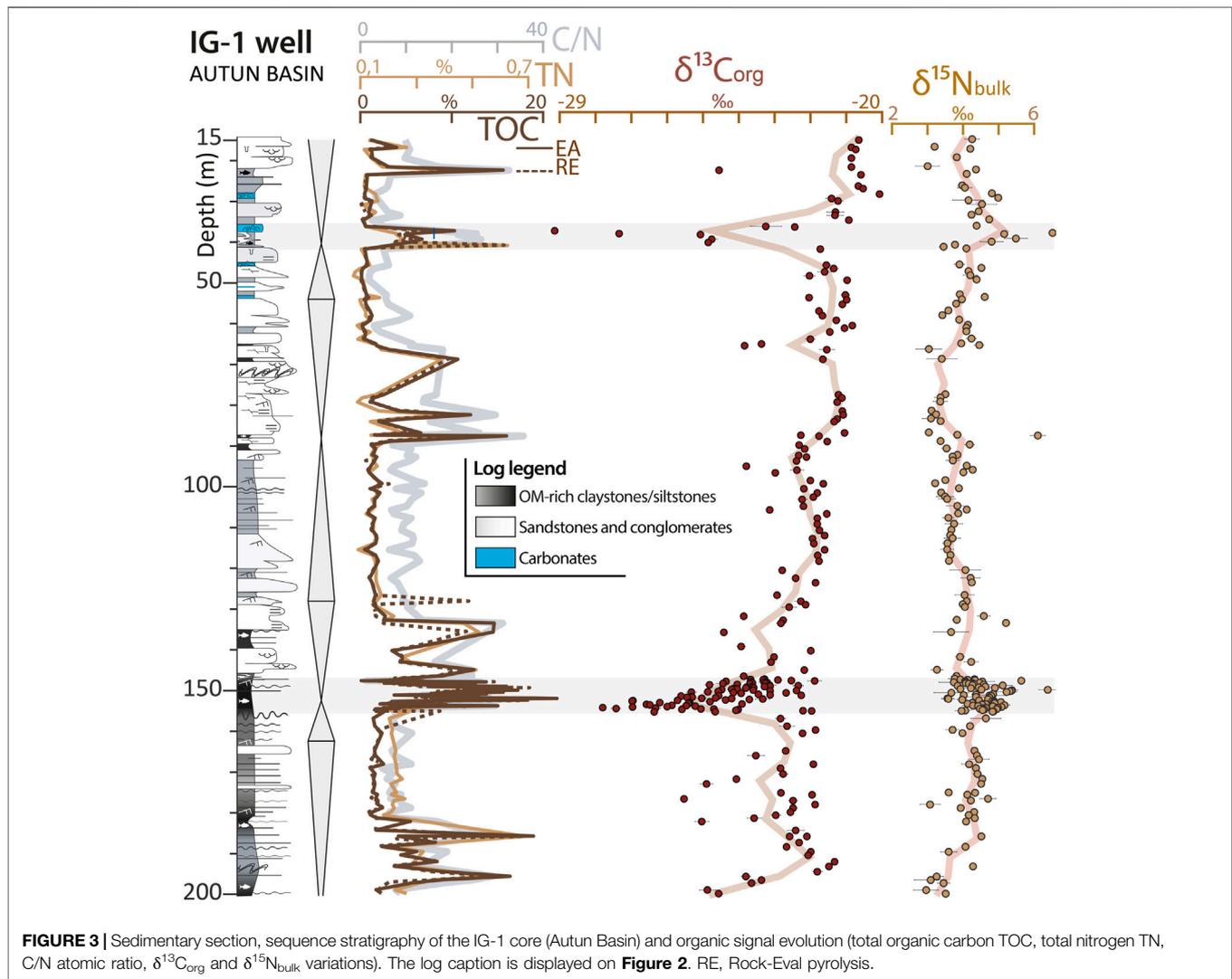In the CHE-1 core, Tmax values range from 413 to 460°C with a mean value of 443 ± 9°C, TOC values range from 0.47 to 12.43 wt.% with a mean value of 2.59 ± 2.40 wt.% (**Figure 4**), HI values range from 22 to 382 mgHC/gTOC with a mean value of 104 ± 88 mgHC/gTOC and OI values range between 4 and 673 mgCO₂/gTOC with a mean value of 99 ± 133 mgCO₂/gTOC (**Supplementary Table 1**). TOC variations (**Figure 4**) fluctuate more than in the IG-1 core record (**Figure 3**). Nonetheless, a first interval of high values (up to 10 wt.%) can be recognized from the base to ~320 m and a second interval from ~240 to 120 m, in which TOC values fluctuate significantly and reach values up to 21 wt.% at 139 m (**Figure 4**).

In the MU core, Tmax values range from 345 to 440°C with a mean value of 418 ± 30°C, TOC values range from 0.18 to 28.03 wt.% with a mean value of 14.01 ± 8.30 wt.% (**Figure 5**), HI values range from 22 to 715 mgHC/gTOC with a mean value of 424 ± 206 mgHC/gTOC and OI values range between 2 and 154 mgCO₂/gTOC with a mean value of 30 ± 47 mgCO₂/gTOC (**Supplementary Table 1**). TOC values are stable around a few percent from the base of the core up to 4 m (**Figure 5**), before progressively increasing up to 30 wt.% at ~2 m. The TOC decreases towards the top of the core with values down to 5 wt.%.

In the SUR section, Tmax values range from 384 to 438°C with a mean value of 423 ± 11°C, TOC values range from 0.06 to 15.82 wt.% with a mean value of 4.55 ± 4.35 wt.% (**Figure 6**), HI values range from 38 to 568 mgHC/gTOC with a mean value of 304 ± 179 mgHC/gTOC and OI values between 3 and 332 mgCO₂/gTOC with a mean value of 33 ± 65 mgCO₂/gTOC (**Supplementary Table 1**). TOC chemostratigraphic variations (**Figure 6**) display 3 peaks of ~10 wt.% at −8 m, ~25 wt.% at 0 m and ~20 wt.% at 7 m.

Palynofacies Analyses

The palynofacies slides selected from the IG-1 core (IG-5, 11, 12, 48, and 54) and from the MU core (MU-3, 5, 13, 14, 15, 24) represent HI values ranging from 100 to up to 700 mgHC/gTOC. In all slides, terrestrial-derived organic particles (phytoclasts, coming from wood tissues), and palynomorphs (spores and pollens, comprising *Botryococcus* algae, as already reported by

FIGURE 3 | Sedimentary section, sequence stratigraphy of the IG-1 core (Autun Basin) and organic signal evolution (total organic carbon TOC, total nitrogen TN, C/N atomic ratio, $\delta^{13}C_{org}$ and $\delta^{15}N_{bulk}$ variations). The log caption is displayed on **Figure 2**. RE, Rock-Eval pyrolysis.

Izart et al., 2012; Garel et al., 2017) are present in varying proportions, but remain quite minor. Amorphous organic matter (AOM) particles, probably algal/bacterial-derived, are the dominant component.
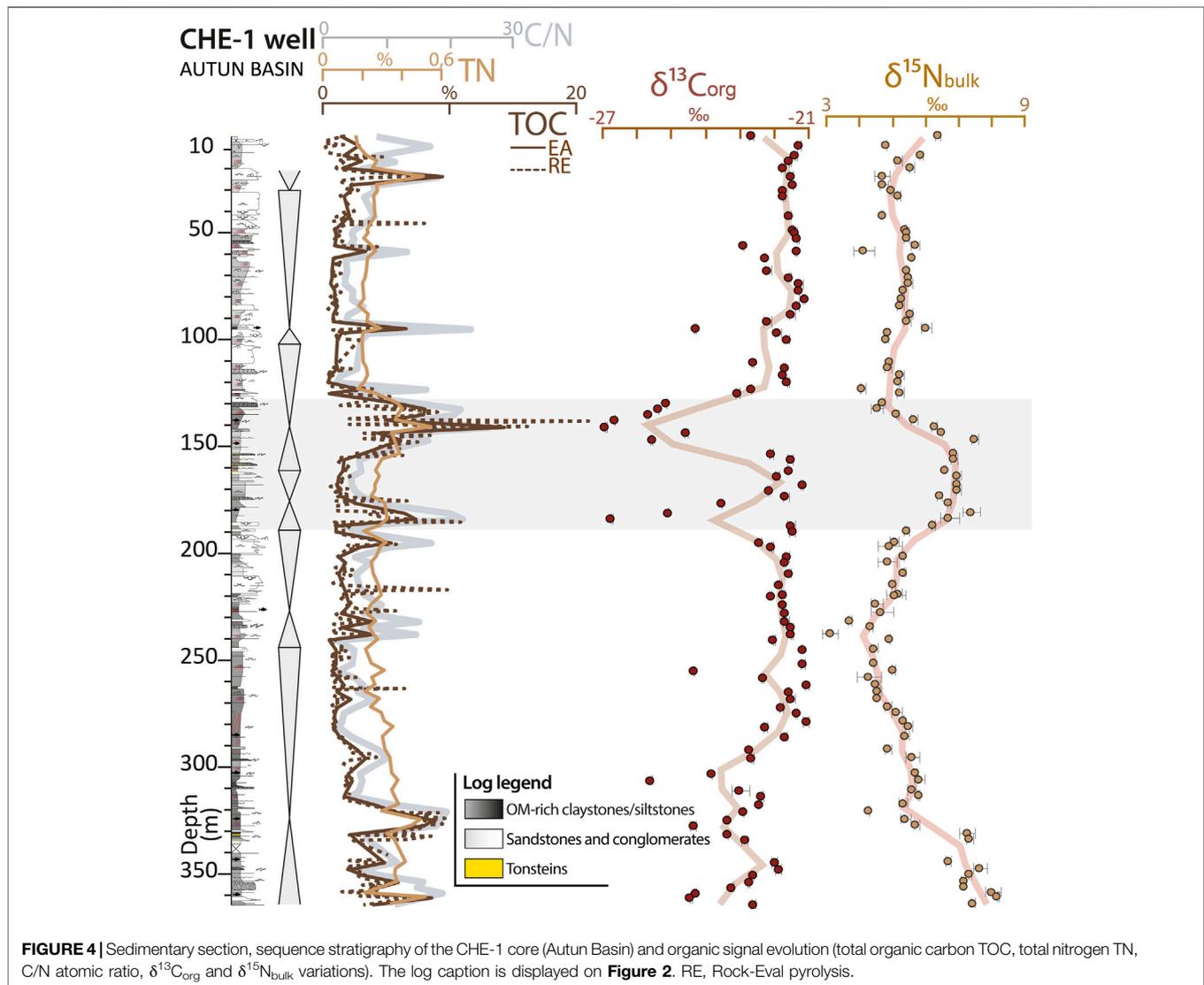
The 10 palynofacies slides selected from CHE-1 core correspond to HI values ranging from 73 to 326 mgHC/gTOC. As in IG-1 and MU cores, a mixture of OM of terrestrial (phytoclasts, palynomorphs) and probably algal-bacterial (AOM) origin is observed (**Figure 7**). Half of the sample set shows AOM particles dominating the terrestrial components (**Figures 7A,B**). The remaining slides show an enhanced composition of organic particles of terrestrial origin (**Figures 7C,D**), suggesting a more contrasted OM source when compared to IG-1 and MU cores.

Elemental and Isotope Geochemical Signals

The TOC content measured with EA-IRMS is consistent with those found by Rock-Eval analyses (**Figure 8**); the R^2 coefficient between TOC values obtained by Rock-Eval pyrolysis and those obtained by elemental analyser is

greater than 0.92 for most of sections, except for the SUR section where an outlier pulls the R^2 coefficient towards lower value ($R^2 = 0.53$, **Figure 8D**).

Total nitrogen (TN) and total organic carbon (TOC) contents are presented in **Figures 3–6, 9** for the different sections (detailed dataset is available on **Supplementary Table 1**). The TN content ranges from 0.07 to 0.76 wt.% in the IG-1 core with a mean value of 0.26 ± 0.14 wt.% (**Figure 3**), from 0.16 to 0.55 wt.% in the CHE-1 core, with a mean value of 0.29 ± 0.08 wt.% (**Figure 4**), from 0.07 to 0.79 wt.% for the MU core, with a mean value of 0.42 ± 0.19 wt.% (**Figure 5**), from 0.15 to 0.68 wt.% for the SUR section, with a mean value of 0.34 ± 0.12 wt.% (**Figure 6**) and from 0.02 to 1.64 wt.% in the LY-F core, with a mean value of 0.47 ± 0.53 wt.% (**Figure 9**). The C/N atomic ratio, calculated from the elemental composition of the organic carbon and total nitrogen, is also shown in **Figures 3–6, 9**. It ranges between 1 and 36 for the IG-1 core, with a mean value of 14 ± 8, between 2 and 26 for the CHE-1 core, with a mean value of 9 ± 6, between 1 and 47 for the MU core, with a mean value of 31 ± 12, between 2 and 42 for the SUR section, with a mean value of 18 ± 14, and between 0 and 86 for the LY-F core, with a mean value of $27 \pm$

FIGURE 4 | Sedimentary section, sequence stratigraphy of the CHE-1 core (Autun Basin) and organic signal evolution (total organic carbon TOC, total nitrogen TN, C/N atomic ratio, $\delta^{13}C_{org}$ and $\delta^{15}N_{bulk}$ variations). The log caption is displayed on **Figure 2**. RE, Rock-Eval pyrolysis.

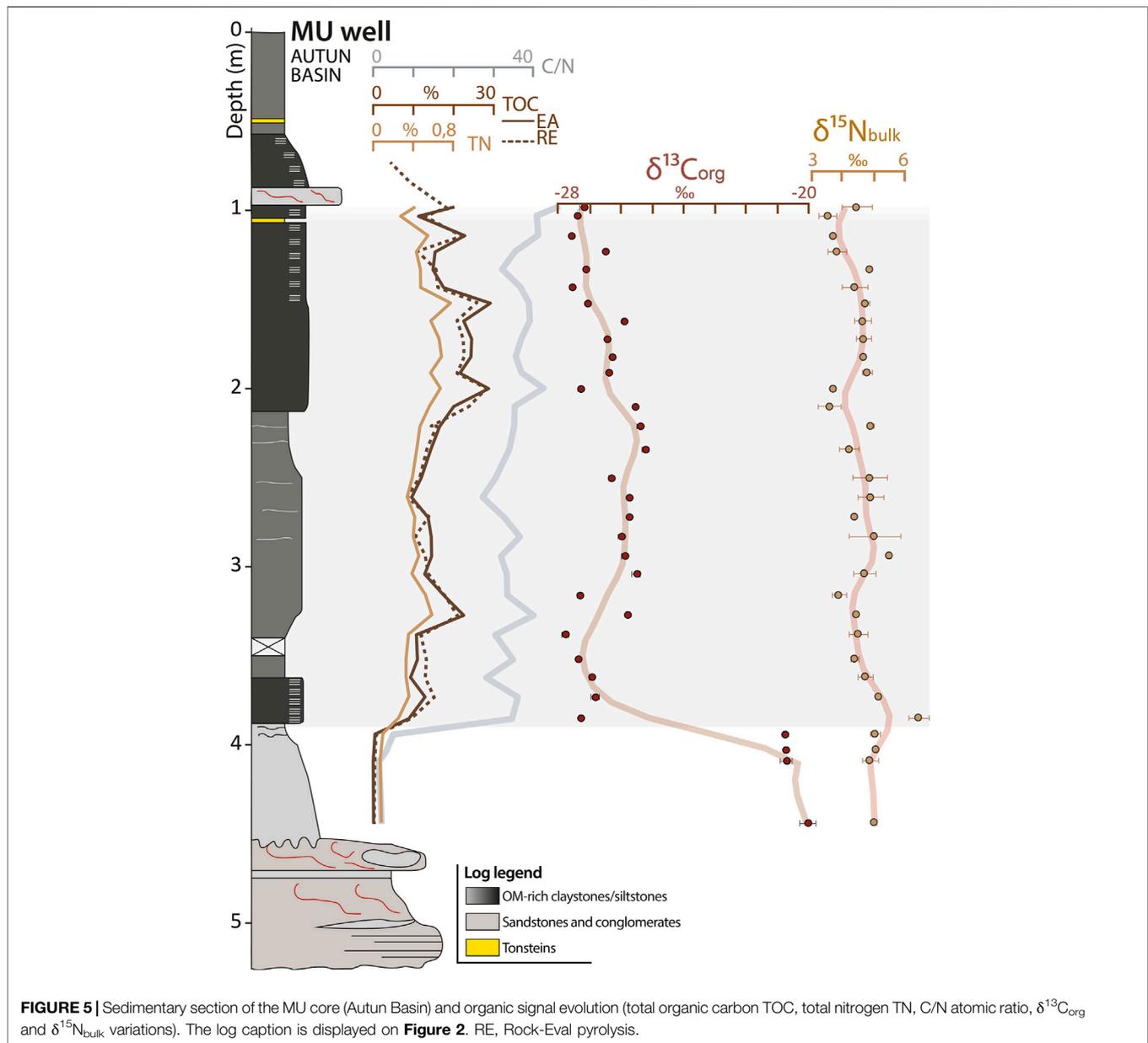18. For each section, C/N variations primarily reflect the TOC evolution.

In the IG-1 core (**Figure 3**), the $\delta^{13}C_{org}$ values gradually increase from −24 to −20‰, with a mean value of −23.1 ± 1.7‰, with large-amplitude negative shifts down to −29.4‰ and −27.3‰ near 150 m (Igornay OSB, clayey facies) and 40 m, respectively. The $\delta^{15}N$ values show less variation, with values ranging from 2.7 to 6.5‰, with a mean value of 4.1 ± 0.62‰. The highest $\delta^{15}N_{bulk}$ values are encountered with the lowest $\delta^{13}C_{org}$, i.e., 6.4‰ close to 150 m and 6.5‰ close to 40 m.

In the CHE-1 core (**Figure 4**), values progressively increase from −24.0 to −21.0‰, with a mean value of −22.5 ± 1.4‰, with negative shifts down to −25.5‰ at ~300 m and −26.8‰ at ~180 m and −27.0‰ at 140 m. These values remain in the same range as those of the IG-1 core. The $\delta^{15}N_{bulk}$ values range from 2.9 to 8.2‰, with a mean value of 5.6 ± 1.1‰, with positive shifts up to 8.3‰ at ~330 m, 7.6‰ at ~190 m and 7.1‰ at ~150 m.

In the MU core, the base is characterized by ^{13}C-enriched OM, with $\delta^{13}C_{org}$ values averaging −20‰, and then sharply dropped by 8‰, down to ~−28‰ all along the core. The $\delta^{15}N_{bulk}$ values present a relatively narrow range from 3.5 to 6.7‰, with a mean value of 4.7 ± 0.7‰ all along the core, with a slight decrease (from 5 to 4‰) towards the top (**Figure 5**).

In the SUR section (**Figure 6**), the $\delta^{13}C_{org}$ curve presents a wavy evolution from −27.5 to −20.6‰, with a mean value of −24.3 ± 2.7‰, and shows a sharp decrease between the cores and the following outcrop at ~−1 m from −20.8 to −26‰. $\delta^{15}N_{bulk}$ values range between 5.3 and 10.1‰, with a mean value of 7.2 ± 1.3‰. The values remain relatively constant (~6‰) up to ~−1 m, with a shift to ~+10‰ at 7 m, followed by a slight decrease towards the top down to ~6‰.

Finally, in the LY-F core (**Figure 9**), $\delta^{13}C_{org}$ values slowly increase from −26.4 to −20‰, with a mean value of −22.2 ± 1.8‰, with two outliers reaching values up to −15.5‰. $\delta^{15}N_{bulk}$ values range from 1 to 4.4‰, with a mean value of

FIGURE 5 | Sedimentary section of the MU core (Autun Basin) and organic signal evolution (total organic carbon TOC, total nitrogen TN, C/N atomic ratio, $\delta^{13}C_{org}$ and $\delta^{15}N_{bulk}$ variations). The log caption is displayed on **Figure 2**. RE, Rock-Eval pyrolysis.

$2.8 \pm 0.7‰$. $\delta^{15}N_{bulk}$ values are stable around 3‰ from the base of the core up to ~400 m, and then show a continuous increase up to ~4.5‰ towards the top of the core.

The dispersion of the elemental results obtained through EA-IRMS are synthesized on **Figure 10** for each section.
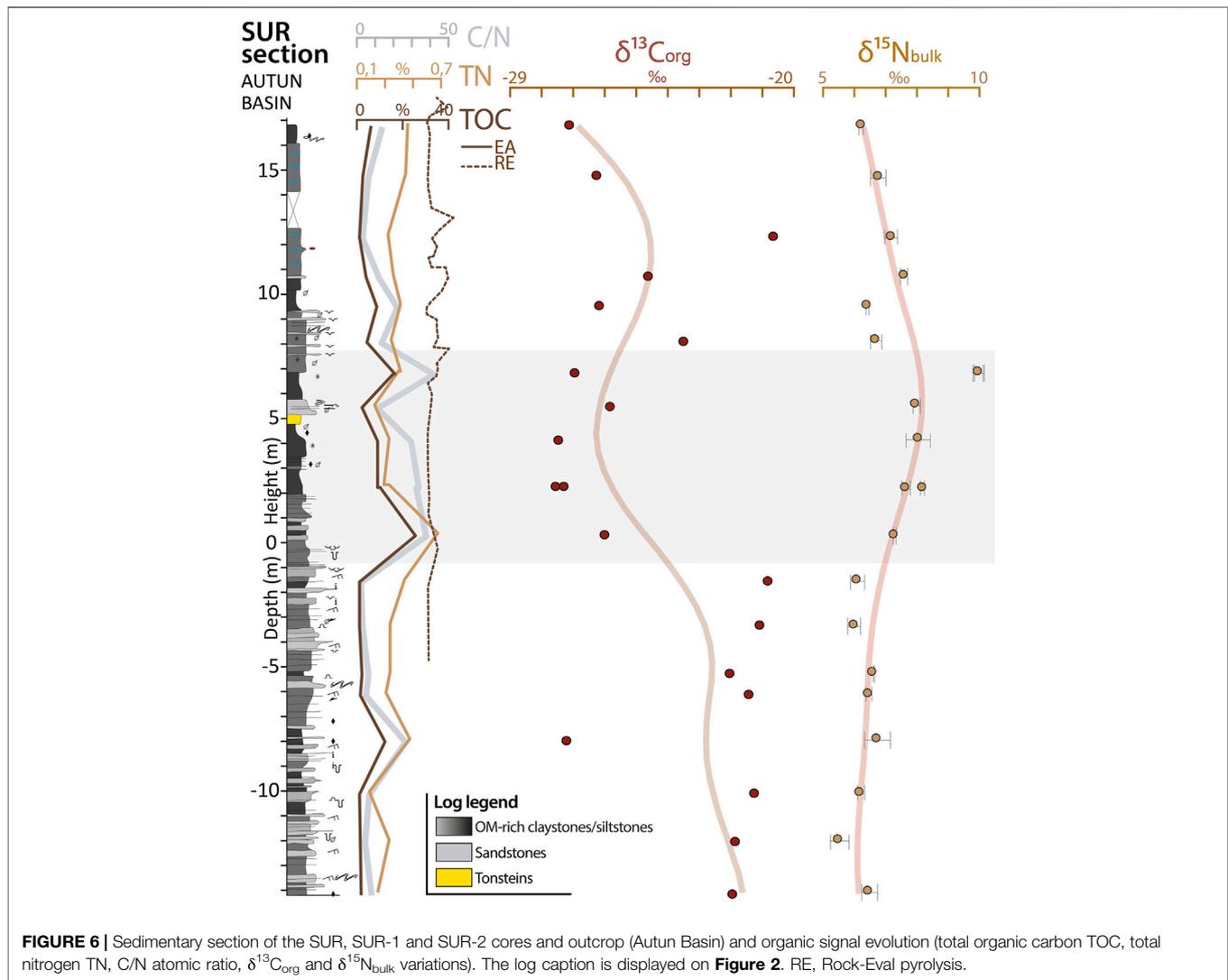
DISCUSSION

Organic-Matter Characterization

Lacustrine sedimentary OM generally consists of a mixture of remains of aquatic primary producers, vascular land plants, palynomorphs and of heterotrophic bacterial biomass thriving in the water column and sediments (Meyers and Ishiwatari,

1995). The OM origin, separated here in autochthonous (i.e., lacustrine algal/bacterial-derived OM) and allochthonous (i.e., terrestrial-derived OM), is appreciated through Rock-Eval pyrolysis results and palynofacies observations. In a lacustrine system such as Autun, AOM is generally considered to originate from primary algal and/or bacterial bio-production in surface waters (Tyson, 1995), whereas in some rarer cases it could have been derived from fixed or floating vegetation installed at the edges of shallow lakes or marshes (Schnyder et al., 2009).

In a pseudo van Krevelen diagram grouping all the sections (**Figure 11**), the HI vs. OI values obtained by Rock-Eval pyrolysis also indicate two types of OM: 1) a Type I OM (autochthonous OM) characterized by high HI and low OI values, and 2) a Type III OM (allochthonous OM) when HI values are low and OI

FIGURE 6 | Sedimentary section of the SUR, SUR-1 and SUR-2 cores and outcrop (Autun Basin) and organic signal evolution (total organic carbon TOC, total nitrogen TN, C/N atomic ratio, $\delta^{13}C_{org}$ and $\delta^{15}N_{bulk}$ variations). The log caption is displayed on **Figure 2**. RE, Rock-Eval pyrolysis.
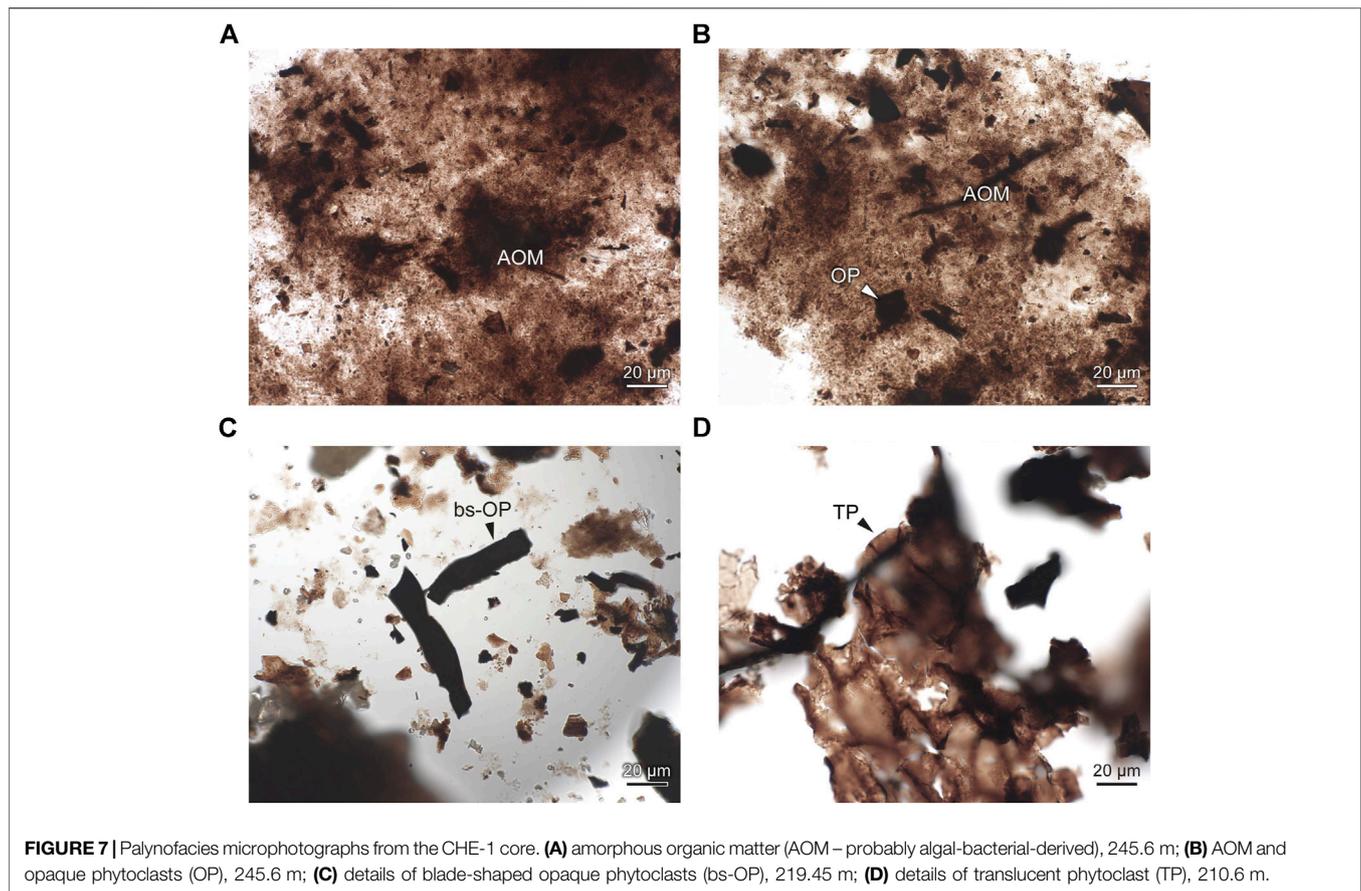
values are high. At the end of the Paleozoic, the Type III OM consists exclusively of vascular land plants with a Calvin-Benson C3 metabolism, the C4 and CAM metabolisms evolving between the Cretaceous and the Tertiary (Thomasson et al., 1986; Bocherens et al., 1993; Cerling, 1999; Kuypers et al., 1999; Sage, 2004). The occurrence of altered Type I OM produced during degradation or oxidation, e.g., under aerobic conditions in the water column, may also explain some of the low HI-high OI endmembers (e.g., Type III, **Figure 11**).

The palynofacies observations confirm the occurrence of mixed sources of OM in the Autun Basin. In most cases, autochthonous AOM seems to predominate over allochthonous terrestrial components in samples with high HI values, notably in IG-1 and MU cores. Intermediate HI and OI values obtained from Rock-Eval mimic a Type II OM (marine OM), but palynofacies observations rather indicate mixture between Type I and Type III. These results are consistent with previous biomarker analyses by gas chromatography mass spectrometry (GC-MS) realized in the Autun Basin, as well as

in the Aumance, Lodève (France) and Saar (Germany) basins by Izart et al. (2012), that reveal a bimodal OM origin (algal and bacterial vs vascular land plants). Moreover, the studies of Doubinger and Elsass (1975), Broutin et al. (1986), Broutin et al. (1990), Becq-Giraudon (1993), conducted in the Autunian facies of the Autun Basin and some other French Massif Central basins, also point out two OM-source endmembers, with fluctuations through time of the vascular land-plant species endmember, depending on their ecology in terms of water needs (i.e. hygrophile vs xerophile plants, well-adapted for wetness and dryness, respectively).
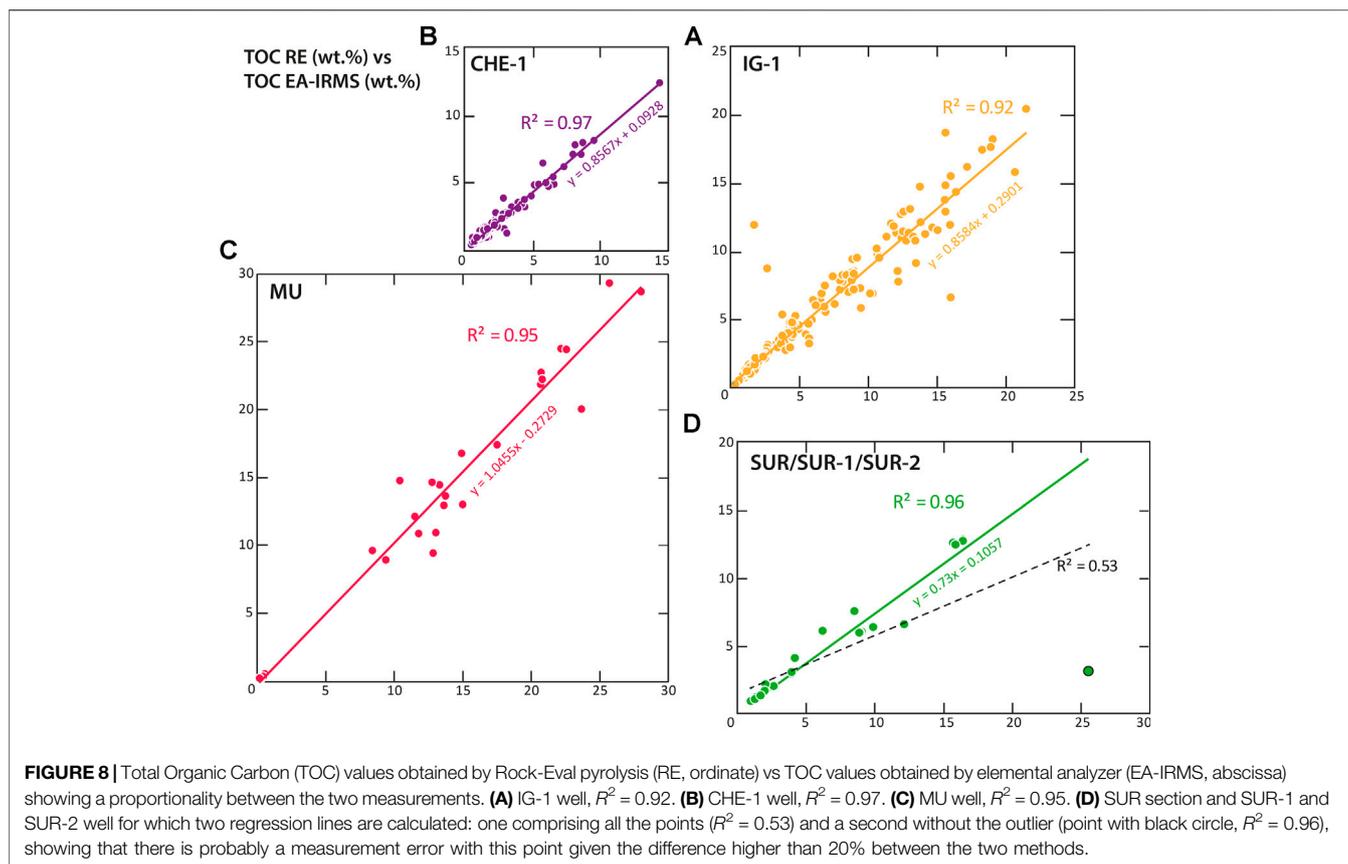
The C/N atomic ratio is usually a good proxy to approximate the OM sources and their relative contribution in lacustrine sediments (Meyers and Ishiwatari, 1993; Meyers, 1994; Meyers and Ishiwatari, 1995; Meyers and Teranes, 2001; Meyers, 2003; Lamb et al., 2006; Birgenheier et al., 2010; Baudin et al., 2017). Indeed, C/N ratios between 4 and 10 characterize autochthonous OM (algae and cyanobacteria, Type I and Type II OM, **Figure 12A**), and values higher than 20 indicate an

FIGURE 7 | Palynofacies microphotographs from the CHE-1 core. **(A)** amorphous organic matter (AOM – probably algal-bacterial-derived), 245.6 m; **(B)** AOM and opaque phytoclasts (OP), 245.6 m; **(C)** details of blade-shaped opaque phytoclasts (bs-OP), 219.45 m; **(D)** details of translucent phytoclast (TP), 210.6 m.

allochthonous source (Type III OM). However, the C/N ratio can be altered over time due to degradation of unstable nitrogen compounds in aquatic OM and the loss of carbon-rich sugars and lipids in terrestrial OM (Lamb et al., 2004). This ratio can be also modified during the earliest diagenesis which tends to decrease the nitrogen content (highly reactive and volatile) and hence increase the C/N ratio (Thomazo et al., 2009). Moreover, this ratio is directly impacted by the presence of mineral nitrogen when nitrogen is measured in bulk material, particularly for samples with a low OM content, where mineral lattice-bound nitrogen (i.e., primarily K-bearing phyllosilicates) can represent a significant fraction of the bulk nitrogen (e.g., Capone et al., 2006). In this study, a fraction of nitrogen (<0.1%) is indeed under fixed form, probably in illite and illite-smectite mixed-layers interlayers as shown by a TN vs. TOC diagram (**Figure 12A**), where the linear regression lines do not intercept the origin of the graph (nitrogen in excess relatively to organic carbon), especially for the MU, LY-F and IG-1 cores. In the case of the MU core, which shows a well-defined regression line (**Figure 12A**), almost 0.1 wt.% of nitrogen is likely fixed in K-bearing minerals, which represents a significant amount (~12%) when compared to the highest value of bulk nitrogen content of ~0.8 wt.%. The nitrogen retention efficiency in K-bearing minerals appears to be even higher in the CHE and SUR sections with 0.2–0.3% of mineral nitrogen (**Figure 12A**), but these values may be biased by poorly-defined regression slopes when compared to other

sections. Moreover, the **Figure 12B** shows an exponential pattern of C/N ratio vs. TOC curves that would not be expected in the absence of mineral nitrogen. Thus, the presence of mineral nitrogen implies that the C/N ratio cannot simply be interpreted in terms of OM sources. In our study, it rather indicates an efficient mechanism of retention of ammonium in K-bearing minerals after the processes of diagenesis and denitrification (i.e., nitrogen loss). Another way to assess the presence of mineral nitrogen in the TN fraction is the C/N values below 1 displayed in the LY-F core, indicating that more nitrogen than carbon is preserved (**Figures 9**, **10**).

For some cores, TN and TOC contents are significantly correlated, such as for the LY-F and MU cores. Such a correlation may suggest an increased input of Type III OM to the aquatic system due to enhanced soil erosion from the lake catchment, associated with a significant clastic input to the lake. However, early diagenetic processes may also be involved in the modification of the sedimentary C/N ratio due to the escape of N_2 during denitrification, leading to a higher C/N ratio (exceeding 10). This remineralization of nitrogen also depends on the type of OM, being highly proteinic and thus N-rich for Type I, while more recalcitrant in case of Type III (highly cellulosic, e.g., Ertel and Hedges, 1985; Meyers, 1994). These two possible interpretations of a sedimentary C/N increase (i.e., variation in nitrogen cycling in the water column or sediments or mixed origin of OM) make a direct

FIGURE 8 | Total Organic Carbon (TOC) values obtained by Rock-Eval pyrolysis (RE, ordinate) vs TOC values obtained by elemental analyzer (EA-IRMS, abscissa) showing a proportionality between the two measurements. **(A)** IG-1 well, $R^2 = 0.92$. **(B)** CHE-1 well, $R^2 = 0.97$. **(C)** MU well, $R^2 = 0.95$. **(D)** SUR section and SUR-1 and SUR-2 well for which two regression lines are calculated: one comprising all the points ($R^2 = 0.53$) and a second without the outlier (point with black circle, $R^2 = 0.96$), showing that there is probably a measurement error with this point given the difference higher than 20% between the two methods.

interpretation of the C/N signal even more confusing (e.g., Van Mooy et al., 2002).

The IG-1 Well (Autun Basin)

Previous Rock-Eval and palynofacies analyses (Elsass-Damon, 1977; Marteau, 1983; Garel et al., 2017) have shown that the OM of Igornay OSB (P2 environment on **Figure 11A**) is mostly composed of a Type I OM. Palynofacies tend to confirm these results, as AOM dominates over phytoclasts and palynomorphs. Very low HI values, such as observed in the delta topset environment (littoral lake L1 environment, **Figure 11A**) could be interpreted as Type III OM input, but palynofacies analyses show generally minor but constant plant-derived components in palynofacies. Thus, low HI values represent more altered Type I OM in proximal environment where the water column is thin, allowing OM degradation by aerobic heterotrophic micro-organisms and the reworking of sediments (which increases sedimentary oxygen depth penetration). Inversely, in the distal environments, OM anaerobic remineralization (including bacterial sulphate reduction and denitrification) is less effective and results in higher TOC contents and higher HI values.

The CHE-1 Well (Autun Basin)

Rock-Eval data show two endmembers, the first one with high HI and low OI values, and conversely a second with low HI and high OI values (**Figure 11B**). This dichotomy may arise from a variable
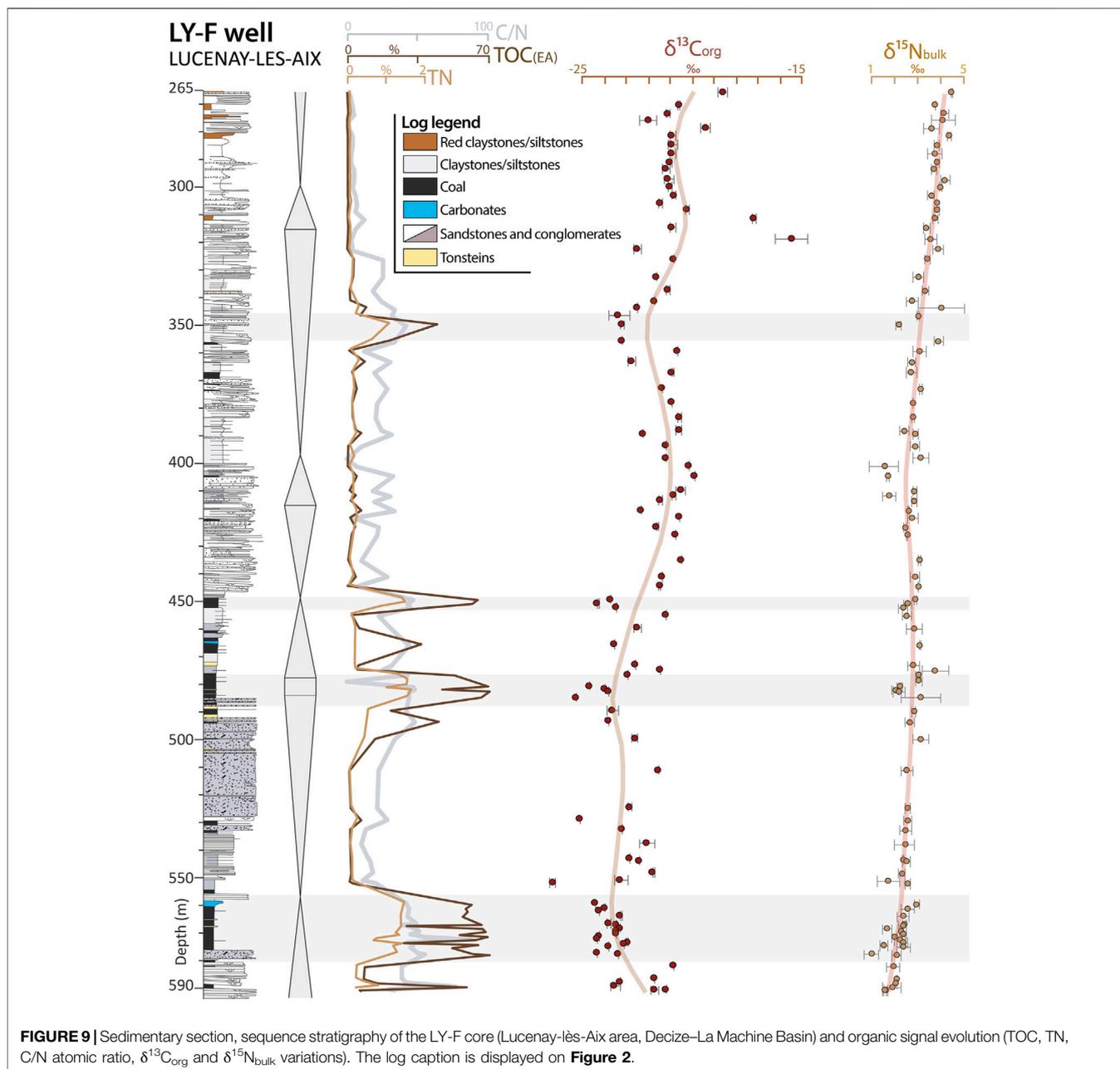
mixture of Type I and a Type III OM or a strongly altered trend in Type I OM after oxidative processes.

The distal-proximal alteration gradient found in the IG-1 core is less distinguishable in the CHE-1 core (**Figure 11B**), as distal lacustrine facies are this time associated with either high or low HI values. The presence of both Type I and Type III OM in distal lacustrine sediments is marked by very variable OI and HI. The palynofacies data indicate that the OM of the CHE-1 core is composed of a mixture of terrestrial-derived and algal/bacterial OM. Judging from our limited palynofacies dataset, the terrestrial component seems higher in CHE-1 when compared to IG-1 and MU cores, which may correspond to lower average HI values, suggesting a higher allochthonous contribution and/or a higher average oxygen level in the water column.

The MU Well (Autun Basin)

As shown by Garel et al. (2017) and this work, Muse OSB (MU well, **Figures 2**, **5**) is composed by a Type I OM with some samples showing a mixture with Type III OM, characterized by gelified OM corresponding to cuticles of land plants. This is confirmed by macroscopic observations showing land plant fragments in the blackest levels. This cuticle-Type III OM has the particularity to present high HI which can reach more than 500 mgHC/gTOC (e.g., Garel et al., 2017), induced by the presence of cuticular wax.

The MU core is composed at its base by proximal environments (from the base to ~4 m, coarse-grained

FIGURE 9 | Sedimentary section, sequence stratigraphy of the LY-F core (Lucenay-lès-Aix area, Decize–La Machine Basin) and organic signal evolution (TOC, TN, C/N atomic ratio, $\delta^{13}C_{org}$ and $\delta^{15}N_{bulk}$ variations). The log caption is displayed on **Figure 2**.

lithologies corresponding to a deltaic topset environment L1 and fine-grained grey lithologies characterising a protected littoral lake environment L2, **Figure 2**), followed by a probable profundal lacustrine P2 environment corresponding to the Muse OSB (from ~4 to 0 m, fine-grained dark lithologies, **Figure 2**). On a pseudo van Krevelen diagram (**Figure 11C**), the distinction between the protected littoral lake and the profundal lake P2 depositional environments is very clear. The OM of the protected littoral lake environment is oxidized compared to those of the profundal lake environment. HI values are not relevant for two of these points because of very low TOC values (<0.25%, **Figure 11C**). However, the macroscopic features of the

protected littoral lake environment level display large land plant fragments, confirming an allochthonous Type III OM, compared to the profundal lake characterized by a dominant autochthonous Type I OM.
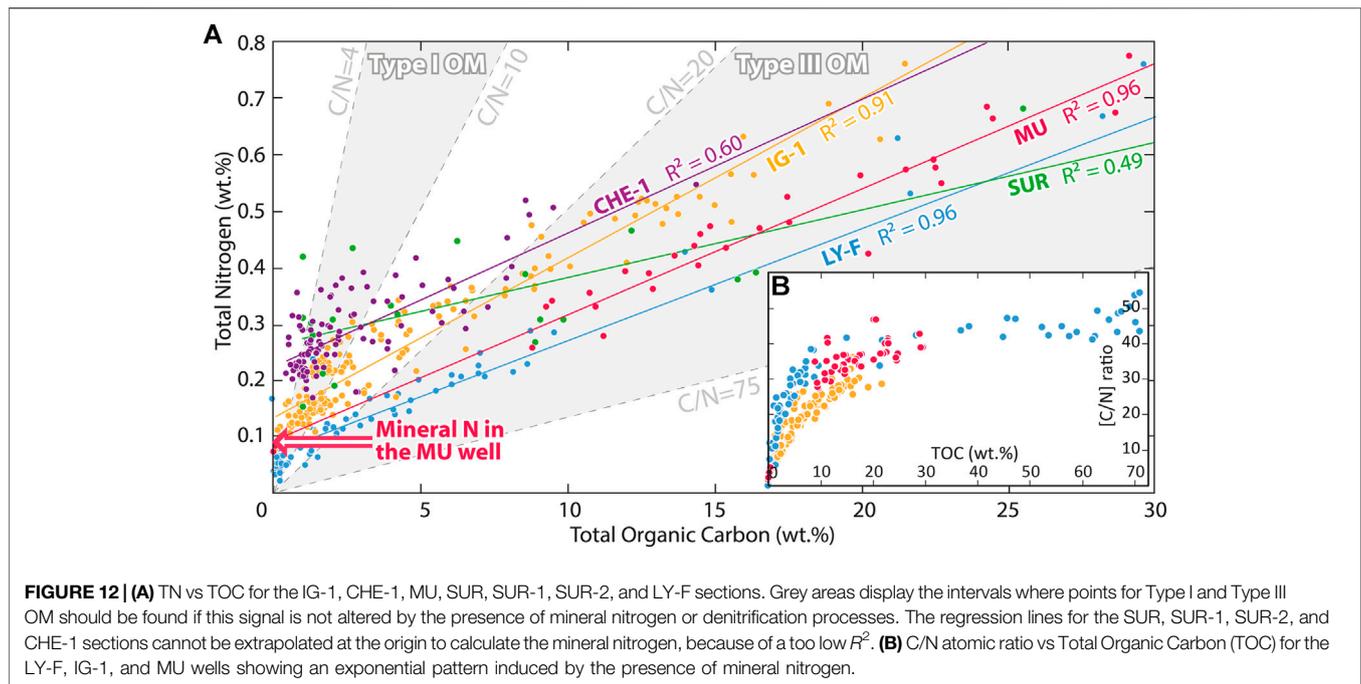
The SUR Section (Autun Basin)

Although very few palynofacies data are available for the SUR section excepted the two samples characterized by Garel et al. (2017), showing that bacterial-derived OM (Type I) is largely dominant, the HI values measured in our study mostly sign a Type I OM (**Figure 11D**). The observed low HI-high OI values could be tentatively assigned to Type III OM, but could also reflect a degraded Type I OM.
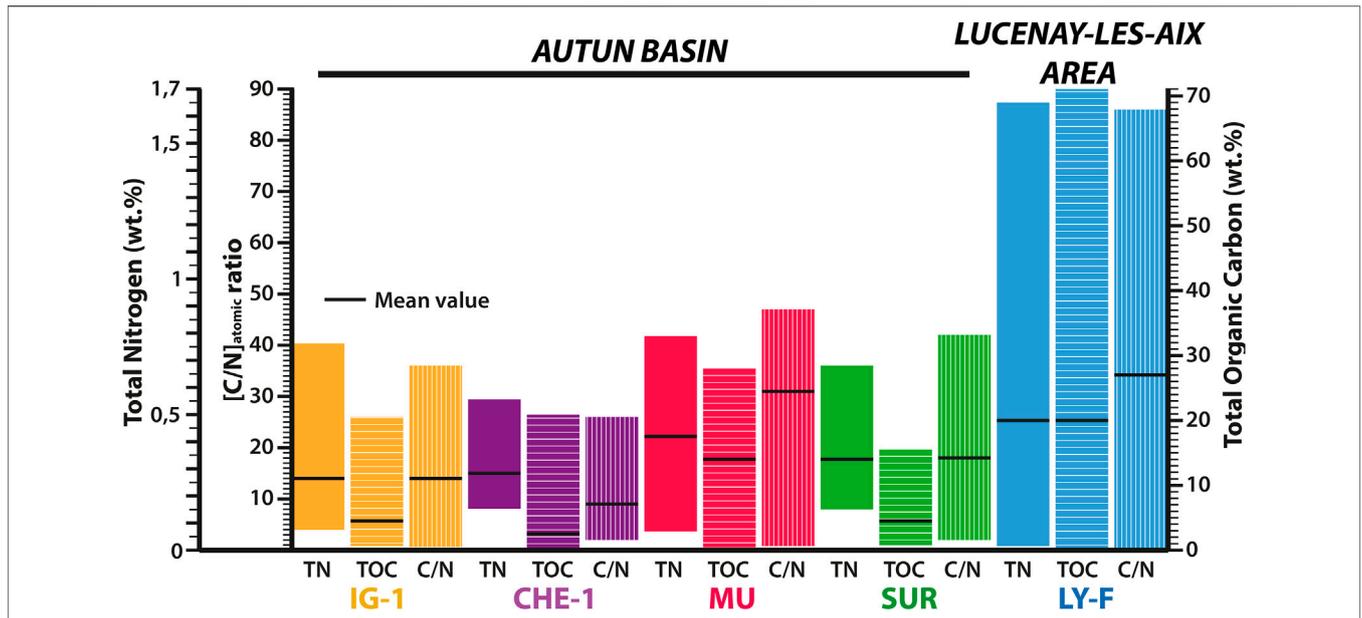
FIGURE 10 | Histograms of the dispersion of total nitrogen (TN), total organic carbon (TOC) and C/N atomic ratio values for all the sections studied; mean values are represented by black horizontal lines; the C and N content is obtained by EA-IRMS. The values display approximatively the same ranges in the Autun Basin, whereas ranges for those of the Lucenay-lès-Aix area are wider.
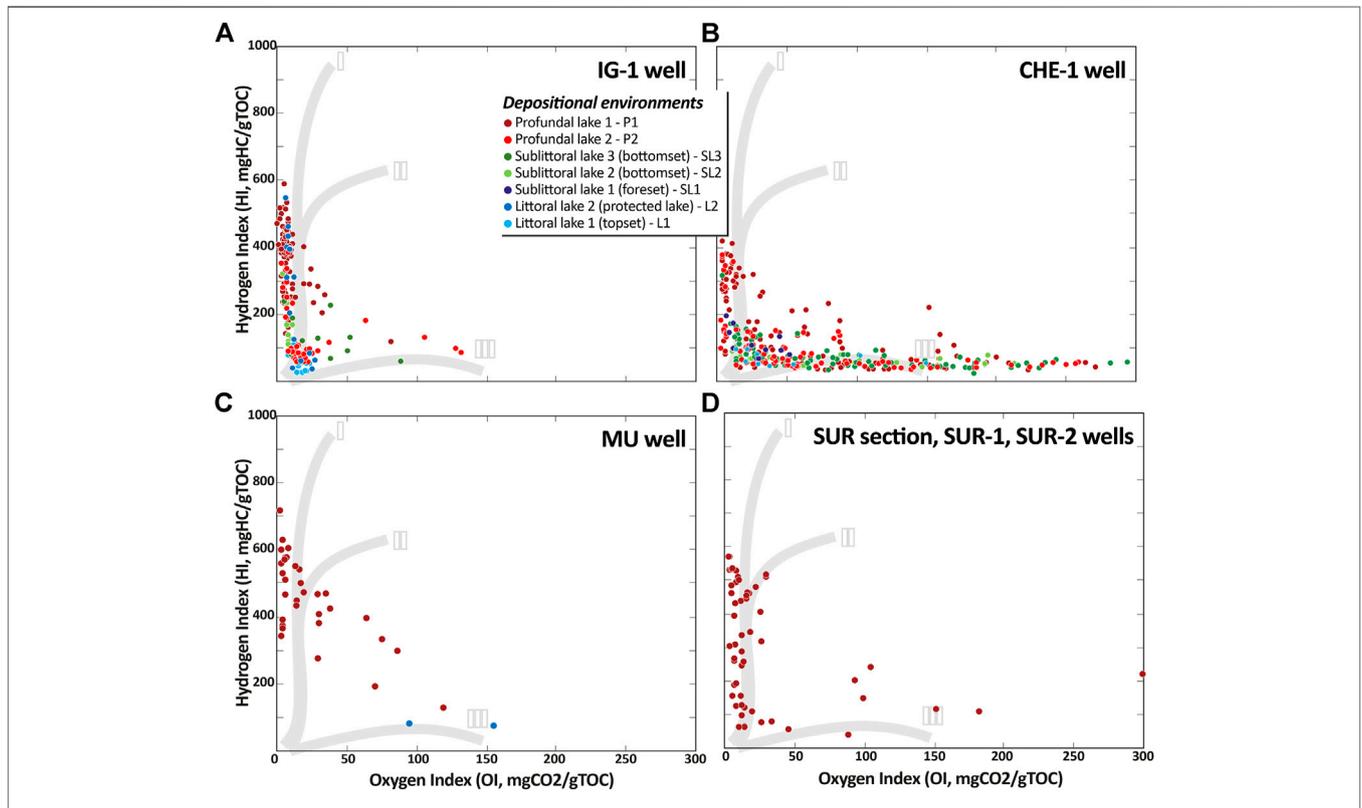
FIGURE 11 | Pseudo-van Krevelen diagrams displaying HI and OI values for the studied section samples depending on the depositional environments. **(A)** In the IG-1 well samples, the more distal facies display the highest HI values, whereas environments submitted to high sediment supply and oxidation processes show lower values. **(B)** In the CHE-1 core samples, the facies distribution is not as marked as for the IG-1 well, with more oxidized samples. **(C,D)** In the MU and SUR cores and section, the environment is only lacustrine (either littoral or profundal) with minimal sediment supply and samples mostly display high HI-low OI values.
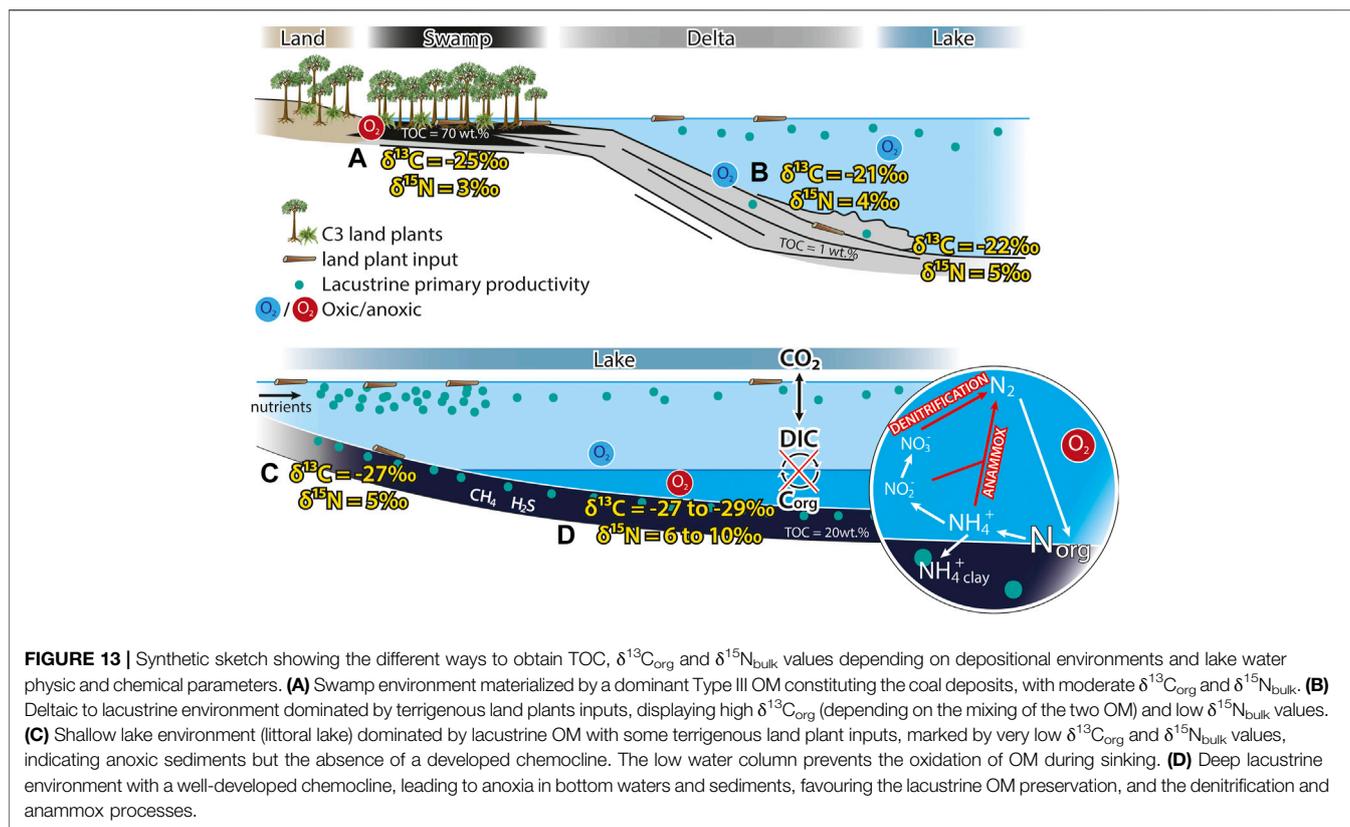
FIGURE 12 | (A) TN vs TOC for the IG-1, CHE-1, MU, SUR, SUR-1, SUR-2, and LY-F sections. Grey areas display the intervals where points for Type I and Type III OM should be found if this signal is not altered by the presence of mineral nitrogen or denitrification processes. The regression lines for the SUR, SUR-1, SUR-2, and CHE-1 sections cannot be extrapolated at the origin to calculate the mineral nitrogen, because of a too low R^2. (B) C/N atomic ratio vs Total Organic Carbon (TOC) for the LY-F, IG-1, and MU wells showing an exponential pattern induced by the presence of mineral nitrogen.

The LY-F Well (Lucenay-lès-Aix Area)

Despite the absence of Rock-Eval pyrolysis and palynofacies data for the LY-F well, the core presents a different geochemical pattern from sections of the Autun Basin. Indeed, this core is composed by an autochthonous lacustrine and allochthonous terrestrial OM mixing, but also by floodplain OM (coal-bearing levels), contrary to the other sections composed dominantly by the mixture of lacustrine and terrestrial OM (**Figures 2, 9**). **Figure 12A** also indicates that mineral nitrogen is present in the samples, but in lower amounts than in the Autun Basin. According to the high $\delta^{13}C_{org}$ values (**Figure 9**), it is likely that allochthonous OM dominates the bulk OM (i.e., the Type I and Type III OM mixing) signal; this core, unlike the sections in the Autun Basin, is dominated by coarse-grained clastic inputs that may indeed contribute a large amount of allochthonous Type III OM to the basin. By comparison, a study in the Western-European Carboniferous to Permian continental Saar-Nahe Basin (Germany, **Figure 1A**) evidenced that such high $\delta^{13}C_{org}$ values (~−21‰) are associated with a dominant Type III OM, based on Rock-Eval and palynofacies analyses, contrary to the Type I OM which is associated to $\delta^{13}C_{org}$ values close to −27‰ (Müller et al., 2006). A similar amplitude between $\delta^{13}C_{org}$ values of autochthonous and allochthonous OM has been observed in an early Cretaceous lacustrine system at Bernissart (Mons Basin, Belgium), were the Type III, allochthonous OM, corresponds to $\delta^{13}C_{org}$ values around −24.5‰, whereas autochthonous primary productivity-derived OM is associated with more negative $\delta^{13}C_{org}$ values, close to −28‰ (Schnyder et al., 2009). The $\delta^{13}C_{org}$ values close to −24‰ for the three coal intervals (i.e. located at ~575, 490, and 450 m in the LY-F well, **Figure 9**) are consistent with $\delta^{13}C_{org}$ values of humic Permian coal from the Australian Sydney Basin (Grice et al., 2007; Ahmed et al., 2009; Retallack et al., 2011).

Preservation of Isotope Organic Signals

Early diagenesis at the sediment-water interface having a low impact on the OM isotope signal preservation (Lehmann et al., 2002), the preservation of OM isotope signal can also be assessed by several parameters: 1) $\delta^{13}C_{org}$ values are consistent with those expected for primary productivity OM (~−25 to −30‰, Schidlowski et al., 1983; Kump and Arthur, 1999), and particularly those expected during this time-window (between −20 and −27%, Strauss and Peters-Kottig, 2003; Müller et al., 2006; Peters-Kottig et al., 2006; Nordt et al., 2016; Cui et al., 2017) and 2) the Tmax parameter, showing values ranging from 423 to 443°C in the studied sections, indicates moderate burial diagenesis. With respect to the petroleum generation, this reflects a relatively immature OM, or at the beginning of the oil window for the highest Tmax values. Moreover, the absence of correlation between the $\delta^{15}N_{bulk}$ and the TN content in all sections shows that the OM isotope signals are probably not pervasively altered by late secondary processes (the nitrogen content being more prone than the carbon to vary during OM alteration, Meyers and Ishiwatari, 1993; Meyers, 2014). Similarly, the $\delta^{15}N_{bulk}$ values obtained are those expected for non-marine sediments, usually between −3 and +7‰ (Peters et al., 1978) and are also within the range of biological signals measured in ancient and modern environments (e.g., Tramoy et al., 2016a; Bouton et al., 2020). $\delta^{13}C_{org}$ negative excursions (**Figures 3–6**) also appear to be of primary origin because diagenesis is expected to induce positive values (Hoefs and Frey, 1976; Monin et al., 1981; Hayes et al., 1983), yet lower than +2‰ (Busigny et al., 2013), and without altering the initial trends (des Marais et al., 1992).

FIGURE 13 | Synthetic sketch showing the different ways to obtain TOC, $\delta^{13}C_{org}$ and $\delta^{15}N_{bulk}$ values depending on depositional environments and lake water physic and chemical parameters. **(A)** Swamp environment materialized by a dominant Type III OM constituting the coal deposits, with moderate $\delta^{13}C_{org}$ and $\delta^{15}N_{bulk}$. **(B)** Deltaic to lacustrine environment dominated by terrigenous land plants inputs, displaying high $\delta^{13}C_{org}$ (depending on the mixing of the two OM) and low $\delta^{15}N_{bulk}$ values. **(C)** Shallow lake environment (littoral lake) dominated by lacustrine OM with some terrigenous land plant inputs, marked by very low $\delta^{13}C_{org}$ and $\delta^{15}N_{bulk}$ values, indicating anoxic sediments but the absence of a developed chemocline. The low water column prevents the oxidation of OM during sinking. **(D)** Deep lacustrine environment with a well-developed chemocline, leading to anoxia in bottom waters and sediments, favouring the lacustrine OM preservation, and the denitrification and anammox processes.

$\delta^{15}N_{bulk}$ Variations

In the modern nitrogen cycle, di-nitrogen (N_2) is withdrawn from the atmosphere during biological fixation by autotrophs as ammonia (NH_3) by the nitrogenase enzyme. Subsequently, the OM sedimentation is followed its mineralization under aerobic or anaerobic conditions with a first step, namely ammonification, consisting in the reduction of organic nitrogen into ammonium (NH_4^+). Then, in aerobic context, NH_4^+ is oxidized to nitrite (NO_2^-) and nitrate (NO_3^-) during nitrification. The produced nitrates can also be biologically assimilated. In anaerobic context (low O_2 in the water column or in sediments, or high sedimentation rates), two processes can occur: anaerobic oxidation of NH_4^+ by an anammox reaction that converts NH_4^+ and NO_2^- to N_2 (**Figure 13**), and denitrification, i.e., a respiratory process that converts NO_3^- to N_2 (Van Mooy et al., 2002; Ader et al., 2016). While nitrification is a moderately fractionating process in modern environments when NH_4^+ oxidation is quantitative, the denitrification pathway is associated with a strong ^{15}N-enrichment of the residual NO_3^-, leading to an increase of $\delta^{15}N_{bulk}$ values owning to the balance between NO_3^- assimilation and N_2 fixation (Peters et al., 1978; Sigman et al., 2009; Ader et al., 2016). Indeed, denitrification induces a fractionation between the residual NO_3^- and released gaseous N_2 and N_2O of about −3‰ in the sediment and up to −25 to −30‰ in the water column (Ader et al., 2016). This process is therefore associated with a ^{15}N-enrichment of the $\delta^{15}N_{bulk}$ values archived in sediments (i.e., positive $\delta^{15}N_{bulk}$ excursions). Similarly, the anammox reaction leads to a ^{15}N-enriched

residual NH_4^+ and so higher $\delta^{15}N_{bulk}$ signal if a sufficient amount of this NH_4^+ is fixed by biological activity or in K-bearing minerals (Prokopenko et al., 2006).

Therefore, positive $\delta^{15}N_{bulk}$ excursions usually indicate an increase in denitrification and/or anammox processes and are associated with the establishment or expansion of strong redox gradient in the water column. Indeed, both processes require chemical stratification of the water column and are often associated with the development of anoxia, at least in the lower part of the water column or in a zone of oxygen minimum in the water column.

In the sedimentary successions studied, positive nitrogen excursions are sometimes associated with increases in TOC and decreases in $\delta^{13}C_{org}$ values, while generally $\delta^{15}N_{bulk}$ and $\delta^{13}C_{org}$ values are not related. Yet, this relation can be explained by several mechanisms under anoxic conditions, including 1) an increase in Type I OM associated with anoxic OM remineralization processes shifting the isotope signal mass balance towards ^{12}C-enriched isotope signal, and/or 2) the build-up of a large dissolved organic carbon reservoir subsequently used by secondary productivity (e.g., Hayes, 1983; Kah et al., 1999; Hayes, 2001; Guo et al., 2013). This coevolution is observed in the IG-1 core in the Igornay OSB at ~155 m and at ~40 m, and also in the CHE-1 core, between ~190 and 130 m. However, periods of high TOC and low $\delta^{13}C_{org}$ values without positive $\delta^{15}N_{bulk}$ excursions (e.g., IG-1 core, ~70 m and MU core, from 4 to 1 m) represent periods when denitrification or anammox processes are absent or less efficient

(i.e., limited to the sediment), indicating that the chemocline is not sustained. This likely indicates a thin water column, promoting the water homogenization, but paired with a substantial primary productivity in surface water, compensating OM degradation during its sinking and before reaching the anoxic sediments, and thus favouring OM-rich deposits. This interpretation is consistent with the protected littoral lake environment (i.e., thin water column) inferred from several sedimentological features for the OM-rich deposits located at ~70 m in the IG-1 core, such as their association with microbial deposits formed in the photic zone (Mercuzot et al., submitted), but differs from the depositional environment inferred for the Muse OSB, firstly considered as deposited in a profundal lake (Mercuzot et al., submitted, based on the classification of Bohacs et al., 2000). These results and interpretations highlight that paired carbon and nitrogen isotope geochemistry can be an additional helpful tool to depositional paleoenvironment determinations, often solely based on sedimentological facies interpretations.

$\delta^{13}C_{org}$ Variations

Whereas the $\delta^{13}C$ of carbonates ($\delta^{13}C_{carb}$) is thought to reflect the $\delta^{13}C$ of the dissolved inorganic carbon (DIC) reservoir, the OM carbon isotope signal ($\delta^{13}C_{org}$) in a lake can be affected by a large combination of factors such as: 1) the isotope composition of the DIC (depending on the isotope composition of the dissolved CO_2 contained in the water compared to atmospheric CO_2), 2) metabolisms of primary producers, their species and growth rates (Mayer and Schwark, 1999), 3) OM sources (allochthonous vs autochthonous, Schnyder et al., 2009; Yans et al., 2010), 4) the water pCO_2 (Herczeg and Fairbanks, 1987), 5) the degradation of particulate organic carbon below the sediment-water interface, 6) the remineralization of dissolved organic carbon in the water column and sediments (e.g., Hayes, 1983; Kah et al., 1999; Hayes, 2001; Guo et al., 2013), and 7) the post-depositional OM thermal decomposition (Strauss et al., 1992; Tocqué et al., 2005; Derry, 2010). Moreover, $\delta^{13}C_{org}$ values in OM-rich environments can be influenced by secondary productivity developing in anoxic bottom waters or within the sediments (e.g., Hayes et al., 1999). In the present study, because of the low burial and the resulting moderate thermal diagenesis state, it is unlikely that $\delta^{13}C_{org}$ variations result from thermal decomposition of OM.
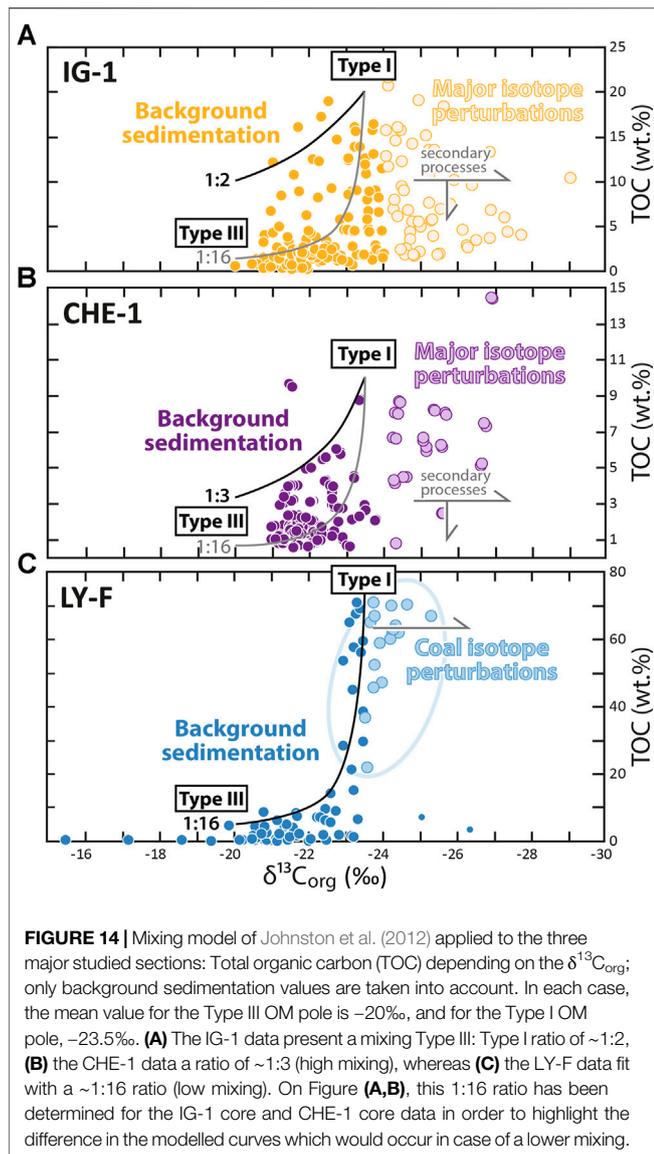
According to the U–Pb dating of the Autun Basin by Pellenard et al. (2017), the sediments from IG-1 and CHE-1 cores are susceptible to have been deposited in less than a million year, revealing high sedimentation rates and thus very short-term $\delta^{13}C_{org}$ variations. The origin of these isotope events is not constrained, but could be related to short-term climate variations, through a direct impact on the lake level and chemistry, or a more indirect impact on sedimentary fluxes, controlling the origin of OM (e.g., terrestrial vs. lacustrine bioproduction, Schnyder et al., 2009; Yans et al., 2010) supplied to the basin.

We considered here that at first order, the $\delta^{13}C_{org}$ variations observed in this study are due to three main parameters: 1) variations of OM sources through time (autochthonous vs.

allochthonous), 2) variations in primary productivity and storage efficiency of OM under a thin water column, or 3) variations in OM remineralization in the water column under a developed chemocline and at the water–sediment interface, associated with fluctuating contribution of secondary heterotrophic biomass to the sedimentary OM. Those parameters may either vary under autocyclic conditions, or be indirectly controlled by climate changes, through fluctuations of the lake level or of the erosion intensity in the catchment area. Furthermore, at second order, these perturbations could also reflect direct climate variations recorded in the basins: in Australian Permian basin, Retallack et al. (2011) have shown that short-term negative carbon excursions in terrestrial OM are synchronous with warmer and wetter "greenhouse crises." This pattern is also observed in United States and South African basins (Retallack, 2013). At a longer time-scale (i.e. 5–7 Myr), $\delta^{13}C_{org}$ variations in bulk OM marine sediments seem to indicate pCO_2 fluctuations, with increases at the beginning of icehouse intervals (ice-caps waxing) and decreases in the second part of the icehouse intervals up to the interglacial (ice-caps waning, Birgenheier et al., 2010). Unfortunately, the pCO_2 evolution is not available through the $\Delta^{13}C$ proxy (i.e., the difference between $\delta^{13}C$ of carbonates and $\delta^{13}C$ of OM), because of the mixing of the OM sources, and the substantial diagenetic overprint on the scarce carbonates preserved in the basins.

Accumulation of OM can be derived from both lacustrine productivity and terrestrial inputs with varying degrees of mixing. In this study, terrigenous OM can even be subdivided into two different origins: one representing the exported terrestrial (allochthonous) OM, the second being direct accumulation of vascular land plants in swamp (i.e., coal). The $\delta^{13}C_{org}$ signature of vascular land plants is evidenced in the coal levels of the Lucenay-lès-Aix area with values around −24‰ (**Figures 9**, **13A**). The remaining $\delta^{13}C_{org}$ variations observed in this study may therefore reflect the interaction of varying degree of mixing between autochthonous productivity and allochthonous OM delivery and secondary processes (e.g., remineralization and secondary productivity). Mixing between OM types with different $\delta^{13}C_{org}$ can be independently inferred based on Rock Eval and palynofacies data, while secondary processes can be evidenced when rapid variations of the $\delta^{13}C_{org}$ are deciphered and cannot be linked to changes in OM types. Within this framework of interpretations, and as supported by the palynofacies data, we observe that periods of low OM accumulation are associated with $\delta^{13}C_{org}$ mean values close to −22‰ (**Figures 3–6**, **9**) and are dominated by Type III OM, and that periods of increasing TOC show ^{12}C-enriched $\delta^{13}C_{org}$ values (down to −29‰) reflecting lake OM production and processing. In addition, OM anaerobic remineralization by bacterial acetotrophic methanogenesis, and to a lesser extent by sulfate reduction, could still lead to lower sedimentary $\delta^{13}C_{org}$ values (Meyers and Ishiwatari, 1995; Müller et al., 2006). However, it can be challenging to distinguish the respective impact of these two secondary processes in the fossil record.

In order to disentangle the various contributions of different sources of OM and the internal lacustrine OM cycling, we explore the relationship between OM-type concentrations and their

FIGURE 14 | Mixing model of Johnston et al. (2012) applied to the three major studied sections: Total organic carbon (TOC) depending on the $\delta^{13}C_{org}$; only background sedimentation values are taken into account. In each case, the mean value for the Type III OM pole is -20‰, and for the Type I OM pole, -23.5‰. **(A)** The IG-1 data present a mixing Type III: Type I ratio of $\sim$1:2, **(B)** the CHE-1 data a ratio of $\sim$1:3 (high mixing), whereas **(C)** the LY-F data fit with a $\sim$1:16 ratio (low mixing). On Figure **(A,B)**, this 1:16 ratio has been determined for the IG-1 core and CHE-1 core data in order to highlight the difference in the modelled curves which would occur in case of a lower mixing.

isotope signals using the concept developed by Johnston et al. (2012) in the following section.

Another Method to Sort $\delta^{13}C_{org}$ Variation Origins?

Common methods have been previously used to constrain the OM types preserved in the sediments of the studied sections, through Rock-Eval pyrolysis interpretations and palynofacies characterization. However, it is difficult to identify secondary cycling OM with this combined method. Johnston et al. (2012) have elaborated a new methodology based on patterns of TOC and ϵ_{TOC} values, the latter approximated here using the $\delta^{13}C_{org}$ signal, to quantitatively infer the respective proportions in a mixture of two OM types (type a and type b). For instance, when a sample consists of a-type and b-type OM in roughly same proportions (i.e., characterized by a a:b ratio close to 1:1), the

TOC vs ϵ_{TOC} (or $\delta^{13}C_{org}$) pattern shows a horizontal straight line. In contrast, when the sample is dominated by one OM type (e.g., 1:100 ratio), the pattern shows an exponential curve. This methodology was applied to our OM data from the longest cores (IG-1, CHE-1, and LY-F wells). The model described the isotopic mass balance of the mixing of two OM sources, based on their respective $\delta^{13}C_{org}$ values (fixed at -20‰ for the Type III OM and at -23.5‰ for the Type I OM), their organic contents (i.e., TOC) and their relative fractions (evolving from 0 to 1, see Johnston et al., 2012 **Supplementary Material** for the detailed equation). The modelled mixing lines are then plotted in the same diagrams than the $\delta^{13}C_{org}$ and TOC measured values, for each well (**Figures 14A–C**). For the IG-1 samples, the best fit corresponds to a Type I: Type III OM ratio close to 1:2 (**Figure 14A**); for the CHE-1 samples, this ratio is close to 1:3 (**Figure 14B**), and for the LY-F, the samples is close to 1:16 (**Figure 14C**). This clearly indicates that in the Autun Basin, during background sedimentation, the OM mixing is composed in nearly equal proportions of Type I and Type III OM, contrary to the Lucenay-lès-Aix Area, where the Type III OM largely dominates the sedimentary OM. Moreover, values departing from the modelled line correspond to the major isotope excursions (i.e., $\delta^{13}C_{org}$ values lower than -23.5‰) recognized in chemostratigraphic profiles. These $\delta^{13}C_{org}$ values are most likely impacted by secondary processes in the case of the IG-1 and CHE-1 samples, that could result from secondary productivity and/or remineralization in anoxic setting.

Therefore, this model seems accurate in identifying and quantify 1) a two-component OM mixing during background sedimentation in the Autun Basin and in the Lucenay-lès-Aix area and 2) punctual isotope excursions reflecting changes in the lake water column functioning, hence expanding the domain of application of this isotope mass balance methodology from Neoproterozoic marine series to Phanerozoic deltaic-lacustrine deposits.

Nitrogen and Carbon Cycling and Depositional Environment Refinement

Considering the exploitable dataset, several cases can be individualized in the two basins studied: 1) periods with $\delta^{13}C_{org}$ values between ~-20 and -22‰, representing the background sedimentation, with a mixture of Type I and Type III OM, sometimes largely dominated by Type III OM as in the Lucenay-lès-Aix area (**Figure 13B**); 2) periods of negative carbon-isotope excursions but not linked with positive nitrogen-isotope excursions, as observed at 70 m in the IG-1 core or in the Muse OSB of the MU core in the Autun Basin (**Figures 3, 5, 13C**); 3) periods where $\delta^{13}C_{org}$ values show sharp negative isotope excursions down to ~-29‰, related to high TOC content and during which positive $\delta^{15}N_{bulk}$ excursions are recorded (Autun Basin).

In the second case (negative $\delta^{13}C_{org}$ excursions only), these periods are attributed to high lacustrine primary productivity in surface waters (represented by high HI values) with a reduced chemocline, in a relatively low water column preventing OM

oxidation during sinking. The bottom waters are not anoxic, within the photic zone, possibly due to the thinness of the water column or the seasonal vertical diffusion of waters observed in some meromictic to polymictic lakes.

In the third case ($\delta^{13}C_{org}$ negative excursions associated with $\delta^{15}N_{bulk}$ positive excursions), these periods are associated with maximum flooding surfaces (MFSs, **Figures 3**, **4**, **9**) and are attributed to reduced OM remineralization under anoxic conditions (minimal sedimentary input and developed chemocline close to the euphotic zone), preventing the equilibrium of the carbon and nitrogen cycles with the atmosphere. Denitrification and/or anammox processes can occur (high $\delta^{15}N_{bulk}$ values), as same as possible sulfate-reduction or methanogenesis (low $\delta^{13}C_{org}$ values, **Figure 13D**). Sometimes, the negative carbon-isotope excursions display a relatively higher duration than their associated positive nitrogen-isotope excursions, at it is the case for the event at ~150 m in the CHE-1 core (**Figure 4**). This pattern was already observed by Algeo et al. (2008), who assume that the recovery of the negative carbon-isotope excursion demands more time than that of the nitrogen positive excursion. In this study, positive nitrogen-isotope excursions are restrained to retrogradational cycles (i.e., periods preceding the MFS) and to MFSs (periods of lowest sediment supply favouring dysoxic/anoxic conditions), and disappear during progradational cycles (i.e., periods following the MFS). By contrast, negative carbon-isotope excursions persist during a part of the progradational cycle, which is also observed in the CHE-1 core between ~150 and 130 m. This can be due to an increasing reoxygenation of the bottom waters when the lake level begins to fall (chemocline demise, high clastic inputs), minimizing denitrification and anammox processes.

The Lucenay-lès-Aix area represents the proximal pole on a depositional environment profile compared to the sections of the Autun Basin, with the presence of supralittoral deposits (coal-bearing sequences deposited in floodplain environments) indicating periods close to the emersion. High $\delta^{13}C_{org}$ values of the enclosing background sedimentation (~−20 to −22‰) indicate the mixture between a lacustrine OM and material derived from terrestrial OM, as observed at a macroscopic scale. However, the Johnston et al. (2012) model previously discussed highlights a higher proportion of Type III OM compare to Type I OM. This feature is consistent with the more proximal depositional environment (i.e., increased terrigenous fluxes) of the Lucenay-lès-Aix area compare to those of the Autun Basin. The coal levels of the Lucenay-lès-Aix area are represented by slight negative carbon-isotope excursions (**Figure 9**) indicating strong OM accumulation and storage of lighter carbon. The $\delta^{15}N_{bulk}$ values do not show significant fluctuations, indicating that the nitrogen cycle is not perturbed, unlike in the Autun OSBs formed in the distal part of the depositional environment profile. Such a geochemical feature is consistent with the absence of a developed chemocline in the environments characterized by very thin water column required for peat accumulation.

Paleoclimate Control

This work shows that it is not simple to assess direct paleoclimate variations from continental late Paleozoic sedimentary successions based solely on OM geochemistry, including carbon and nitrogen isotopes, Rock-Eval and palynofacies analyses, as these signals are highly affected by OM-sources and autocyclic and secondary processes (e.g., variations in intensity of the primary productivity, secondary productivity overprint, OM remineralization). Moreover, in the context of the European Permian basins, the high sedimentation rates (e.g., 300 m/Ma in the Saar-Nahe Basin, Stollhofen et al., 1999), probably linked to the dismantling of the Variscan belt, induce fast-changing depositional environments along the sedimentary sections, thus adding complexity to record and decipher long-term paleoclimate modifications.

Although the infilling of European Carboniferous to Permian basins is synchronous of the peak icehouse period of the LPIA (Crowley and Baum, 1992; Isbell et al., 2003; Montañez et al., 2007; Fielding et al., 2008; Isbell et al., 2012; Montañez and Poulsen, 2013; Soreghan et al., 2019), some of them record relatively short-term climate variations. Retallack (2013) evidenced two "greenhouse crises" during the Asselian, associated with increasing global temperatures and precipitations. Roscher and Schneider (2006) suggest wet phases during late Carboniferous and Permian in Europe, including one at the base of the Asselian, also recognized by Trümper et al. (2020) in Germany. Retallack et al. (2011) also indicate that negative $\delta^{13}C_{org}$ excursions in Australian Permian sediments are synchronous with warmer and wetter periods. In the Autun Basin, palynology analyses of Doubinger and Elsass (1975) indicate alternating wet and dry periods during the whole filling of the basin. However, these climate variations are likely occurring at longer time scale than the carbon and nitrogen isotope trends presented in our study, but it seems that some shorter-term climate modifications can also be inferred from our sedimentary successions, when 1) taking into account sequence stratigraphy features, and 2) comparing our dataset to previous studies and discussions.

In the Autun Basin, OSBs correspond to maximum flooding intervals, underpinning an increase in the relative lake level, either due to 1) a subsidence increase (i.e., tectonic-control hypothesis), or 2) wetter periods (i.e. climate-control hypothesis). Given the radiometric ages obtained for the lower Autunian in the Autun Basin by Pellenard et al. (2017), the whole studied sedimentary successions of IG-1 and CHE-1 wells necessarily correspond to a time-interval shorter than 10^6 yr, thus reflecting geochemical perturbations within a range of ~10^5 yr. As tectonic processes occur on a longer time scale (10^6–10^8 yr), the subsidence hypothesis appears unlikely, and climate forcing may thus explain part of the lake-level variations and OM-rich level deposits. Moreover, the results of cyclostratigraphy tests, notably performed on the TOC values of the CHE-1 core, show a cyclic pattern (Schnyder et al., 2020), that would suggest that the OM accumulation and the local and secondary processes may have been indirectly controlled by climate variations. Such an hypothesis is consistent with the work of Izart et al. (2012), who analyzed biomarkers in several

Carboniferous to Permian European basins, and shown that in the Autun and Saar-Nahe basins, δD values of mid- and long-chain n-alkanes coming from vascular land plants are higher than δD values of short-chain n-alkanes coming from algal OM. This pattern, also discussed in modern and recent sediments, in the Jurassic and in the late Paleozoic (Dawson et al., 2004; Sachse et al., 2004; Tramoy et al., 2016b), seems to indicate that black shales deposits would form during wetter periods occurring in an overall dry tropical, i.e., during more sustained monsoonal episodes, thus linking OM-rich deposits with wet climate episodes. A high-resolution dedicated study on deuterium isotope of biomarkers in the Autun and Decize–La Machine basins may therefore represent an interesting perspective.

CONCLUSION

This study evidences perturbations in the carbon and nitrogen cycles in the late Carboniferous to early Permian Autun and Decize–La Machine continental basins located in the eastern Pangea. These biogeochemical variations have been attributed to diverse physical and chemical lacustrine conditions in relation with depositional environments. At first order, increases in TOC and TN contents are associated with periods of enhanced OM storage in sediments during high lake level events. These events are accompanied by negative carbon-isotope excursions, and sometime positive nitrogen-isotope excursions. Long-term variations in $\delta^{13}C_{org}$ values indicate changes in OM sources to the basin through time, with very low values (~−29 to −23.5‰) associated with *in-situ* lacustrine production (autochthonous Type I OM) and higher values (~−22 to −20‰) with terrestrial input (allochthonous Type III OM). This interpretation is consistent on a regional scale (i.e., when comparing with the contemporaneous German Saar-Nahe Basin). Variations of the $\delta^{15}N_{bulk}$ signal inform on the chemical stratification of the water column, with high values reflecting denitrification or anammox processes occurring in anoxic water bodies, below a well-developed chemocline. Associated with black shale deposits, this water stratification prevents the equilibrium between the $\delta^{13}C$ of the dissolved carbon in bottom waters and the $\delta^{13}C$ of the atmospheric CO_2. This feature is due to the secondary productivity metabolisms driving the low $\delta^{13}C_{org}$ signal of anoxic sediments (probable bacterial methanogenesis and/or sulfate reduction).

Low sedimentary $\delta^{13}C_{org}$ values associated with constant $\delta^{15}N_{bulk}$ values indicate periods of high primary productivity of surface waters and spatially-decoupled nitrogen and carbon cycles (i.e., the nitrogen cycle recording the water column processes while the carbon cycle records sedimentary processes and diagenesis imprints). For more proximal environments (i.e., swamps in floodplain environments), negative $\delta^{13}C_{org}$ excursions are explained by Type III OM accumulation as coal deposits.

Finally, this work demonstrates that in lake-dominated paleoenvironments, global paleoclimate reconstructions based on organic carbon and nitrogen biogeochemical cycles can only be attempted when the OM source mixing and the secondary processes (i.e., occurring in the water column and the sediments and linked to various internal factors) are precisely determined, and that geochemically-based interpretations can help to detail or refine previous sedimentologically-based paleoenvironment reconstructions. Even if some studies indicate that negative carbon-isotope excursions can be accounted during wetter climate intervals, and therefore that the imprint of climate was probable on OM sedimentation in the Autun and Decize-La Machin basins, complementary methods should be used to deconvolute in detail the influence of OM origins and water-column reprocessing on the C and N sedimentary isotope signals, linked to local controls, from climate variations.

DATA AVAILABILITY STATEMENT

The original contributions presented in the study are included in the article/**Supplementary Material**, further inquiries can be directed to the corresponding author.

AUTHOR CONTRIBUTIONS

MM, PP, JS, FB, A-CP-W, MBu, and LG collected the samples and realized geochemical analyses with TM, AS, MBo, and TB. A-LS managed the analytical process. PS-J helped with core-drilling process. MM, CT, JS, PP, SB, LB, GG, MBu, and LG contributed to sedimentological and stratigraphical descriptions of the sections. MM and CT wrote the manuscript with inputs from all authors. All authors contributed to the interpretation of the data and approved the submitted version.

FUNDING

ACKNOWLEDGMENTS

SUPPLEMENTARY MATERIAL

The Supplementary Material for this article can be found online at: https://www.frontiersin.org/articles/10.3389/feart.2021.705351/full#supplementary-material

REFERENCES

Ader, M., Sansjofre, P., Halverson, G. P., Busigny, V., Trindade, R. I. F., Kunzmann, M., et al. (2014). Ocean Redox Structure Across the Late Neoproterozoic Oxygenation Event: A Nitrogen Isotope Perspective. *Earth Planet. Sci. Lett.* 396, 1–13. doi:10.1016/j.epsl.2014.03.042

Ader, M., Thomazo, C., Sansjofre, P., Busigny, V., Papineau, D., Laffont, R., et al. (2016). Interpretation of the Nitrogen Isotopic Composition of Precambrian Sedimentary Rocks: Assumptions and Perspectives. *Chem. Geol.* 429, 93–110. doi:10.1016/j.chemgeo.2016.02.010

Ahmed, M., Volk, H., George, S. C., Faiz, M., and Stalker, L. (2009). Generation and Expulsion of Oils from Permian Coals of the Sydney Basin, Australia. *Org. Geochem.* 40, 810–831. doi:10.1016/j.orggeochem.2009.04.003

Algeo, T., Rowe, H., Hower, J. C., Schwark, L., Herrmann, A., and Heckel, P. (2008). Changes in Ocean Denitrification During Late Carboniferous Glacial-Interglacial Cycles. *Nat. Geosci.* 1, 709–714. doi:10.1038/ngeo307

Altabet, M. A., and Francois, R. (1994). Sedimentary Nitrogen Isotopic Ratio as a Recorder for Surface Ocean Nitrate Utilization. *Glob. Biogeochem. Cycles* 8, 103–116. doi:10.1029/93GB03396

Batten, D. J. (1982). Palynofacies, Palaeoenvironments and Petroleum. *J. Micropalaeontol.* 1, 107–114. doi:10.1144/jm.1.1.107

Baudin, F., Tribovillard, N., and Trichet, J. (2017). *Géologie de la matière organique.* Les Ulis: EDP Sciences.

Beauchamp, B., Oldershaw, A. E., and Krouse, H. R. (1987). Upper Carboniferous to Upper Permian 13C-Enriched Primary Carbonates in the Sverdrup basin, Canadian Arctic: Comparisons to Coeval Western North American Ocean Margins. *Chem. Geology. Isotope Geosci. section* 65, 391–413. doi:10.1016/0168-9622(87)90016-9

Beccaletto, L., Capar, L., Serrano, O., and Marc, S. (2015). Structural Evolution and Sedimentary Record of the Stephano-Permian Basins Occurring beneath the Mesozoic Sedimentary Cover in the Southwestern Paris Basin (France). *Bull. Soc. Géol. Fr.* 186, 429–450. doi:10.2113/gssgfbull.186.6.429

Becq-Giraudon, J.-F., Montenat, C., and Van Den Driessche, J. (1996). Hercynian High-Altitude Phenomena in the French Massif Central: Tectonic Implications. *Palaeogeogr. Palaeoclimatol. Palaeoecol.* 122, 227–241. doi:10.1016/0031-0182(95)00081-X

Becq-Giraudon, J.-F. (1993). Problèmes de la biostratigraphie dans le Paléozoïque supérieur continental (Stéphanien - Autunien) du Massif Central. *Geodinamica Acta* 6, 219–224. doi:10.1080/09853111.1993.11105249

Behar, F., Beaumont, V., and De B. Penteado, H. L. (2001). Rock-Eval 6 Technology: Performances and Developments. *Oil Gas Sci. Technol.* 56, 111–134. doi:10.2516/ogst:2001013

Berner, R. A. (2001). "The Effect of the Rise of Land Plants on Atmospheric CO2 During the Paleozoic," in *Plants Invade the Land: Evolutionary and Environmental Perspectives.* Editors P. G. Gensel and D. Edwards (New York, NY: Columbia University Press), 173–178.

Berner, R. A. (1989). Biogeochemical Cycles of Carbon and Sulfur and Their Effect on Atmospheric Oxygen Over Phanerozoic Time. *Glob. Planet. Change* 1, 97–122. doi:10.1016/0921-8181(89)90018-0

Berner, R. A., and Canfield, D. E. (1989). A New Model for Atmospheric Oxygen over Phanerozoic Time. *Am. J. Sci.* 289, 333–361. doi:10.2475/ajs.289.4.333

Berner, R. A., and Raiswell, R. (1983). Burial of Organic Carbon and Pyrite Sulfur in Sediments over Phanerozoic Time: a New Theory. *Geochim. Cosmochim. Acta* 47, 855–862. doi:10.1016/0016-7037(83)90151-5

Berner, R. A. (2003). The Long-Term Carbon Cycle, Fossil Fuels and Atmospheric Composition. *Nature* 426, 323–326. doi:10.1038/nature02131

Birgenheier, L. P., Frank, T. D., Fielding, C. R., and Rygel, M. C. (2010). Coupled Carbon Isotopic and Sedimentological Records from the Permian System of Eastern Australia Reveal the Response of Atmospheric Carbon Dioxide to Glacial Growth and Decay during the Late Palaeozoic Ice Age. *Palaeogeogr. Palaeoclimatol. Palaeoecol.* 286, 178–193. doi:10.1016/j.palaeo.2010.01.008

Bocherens, H., Friis, E. M., Mariotti, A., and Pedersen, K. R. (1993). Carbon Isotopic Abundances in Mesozoic and Cenozoic Fossil Plants: Palaeoecological Implications. *Lethaia* 26, 347–358. doi:10.1111/j.1502-3931.1993.tb01541.x

Bohacs, K. M., Carroll, A. R., Neal, J. E., and Mankiewicz, P. J. (2000). Lake-Basin Type, Source Potential, and Hydrocarbon Character: An Integrated Sequence-Stratigraphic-Geochemical Framework," in *Lake Basins Through Space and Time*. Editors Gierlowski-Kordesch, E. H., and Kelts, K. (American Association of Petroleum Geologists), 3–34.

Bouton, A., Vennin, E., Thomazo, C., Mathieu, O., Garcia, F., Jaubert, M., et al. (2020). Microbial Origin of the Organic Matter Preserved in the Cayo Coco Lagoonal Network, Cuba. *Minerals* 10, 143. doi:10.3390/min10020143

Broutin, J., Doubinger, J., Farjanel, G., Freytet, P., Kerp, H., Langiaux, J., et al. (1990). Le renouvellement des flores au passage Carbonifère Permien: approches stratigraphique, biologique, sédimentologique. *Comptes Rendus de l'Académie des Sci. Paris* 311, 1563–1569.

Broutin, J., Doubinger, J., Langiaux, J., and Primey, D. (1986). Conséquences de la coexistence de flores à caractères stéphaniens et autuniens dans les bassins limniques d'Europe occidentale. *Mémoires de la Société Géologique de France Nouvelle Série* 149, 15–25.

Bruckschen, P., Oesmann, S., and Veizer, J. (1999). Isotope Stratigraphy of the European Carboniferous: Proxy Signals for Ocean Chemistry, Climate and Tectonics. *Chem. Geology.* 161, 127–163. doi:10.1016/S0009-2541(99)00084-4

Burg, J. P., Brun, J. P., and Van Den Driessche, J. (1990). "Le sillon houiller du Massif Central français: faille de transfert pendant l'amincissement crustal de la chaîne," in *Comptes rendus de l'Académie des sciences. Série 2, Mécanique, Physique, Chimie, Sciences de l'univers, Sciences de la Terre*, 147–152.

Burg, J. P., van den Driessche, J., and Brun, J. P. (1994). Syn-to post-thickening Extension in the Variscan Belt of Western Europe: Modes and Structural Consequences. *Géologie de la France* 3, 33–51.

Busigny, V., Lebeau, O., Ader, M., Krapež, B., and Bekker, A. (2013). Nitrogen Cycle in the Late Archean Ferruginous Ocean. *Chem. Geol.* 362, 115–130. doi:10.1016/j.chemgeo.2013.06.023

Capone, D. G., Popa, R., Flood, B., and Nealson, K. H. (2006). GEOCHEMISTRY: Follow the Nitrogen. *Science* 312, 708–709. doi:10.1126/science.1111863

Cerling, T. E. (1999). "Paleorecords of C4 Plants and Ecosystems," in *Paleorecords of C4 Plants and Ecosystems*. Editors R. F. Sage and R. K. Monson (San Diego, CA: Academic Press), 445–469.

Choulet, F., Faure, M., Fabbri, O., and Monié, P. (2012). Relationships between Magmatism and Extension along the Autun-La Serre Fault System in the Variscan Belt of the Eastern French Massif Central. *Int. J. Earth Sci.* 101, 393–413. doi:10.1007/s00531-011-0673-z

Cleal, C. J., and Thomas, B. A. (2005). Palaeozoic Tropical Rainforests and Their Effect on Global Climates: Is the Past the Key to the Present?. *Geobiology* 3, 13–31. doi:10.1111/j.1472-4669.2005.00043.x

Combaz, A. (1964). Les Palynofaciès. *Revue de Micropaléontologie* 7, 205–218.

Crowley, T. J., and Baum, S. K. (1992). Modeling Late Paleozoic Glaciation. *Geology* 20, 507–510. doi:10.1130/0091-7613(1992)020<0507:MLPG>2.3.CO;2

Cui, Y., Bercovici, A., Yu, J., Kump, L. R., Freeman, K. H., Su, S., et al. (2017). Carbon Cycle Perturbation Expressed in Terrestrial Permian-Triassic Boundary Sections in South China. *Glob. Planet. Change* 148, 272–285. doi:10.1016/j.gloplacha.2015.10.018

Dawson, D., Grice, K., Wang, S. X., Alexander, R., and Radke, J. (2004). Stable Hydrogen Isotopic Composition of Hydrocarbons in Torbanites (Late Carboniferous to Late Permian) Deposited under Various Climatic Conditions. *Org. Geochem.* 35, 189–197. doi:10.1016/j.orggeochem.2003.09.004

Derry, L. A. (2010). On the Significance of δ13C Correlations in Ancient Sediments. *Earth Planet. Sci. Lett.* 296, 497–501. doi:10.1016/j.epsl.2010.05.035

des Marais, D. J., Strauss, H., Summons, R., and Hayes, J. M. (1992). The Proterozoic Carbon Isotopic Record of Organic Burial Rates, Changing Redox Conditions and Atmospheric CO2 Levels. Cincinnati: Geological Society of America.

Deutsch, C., Sigman, D. M., Thunell, R. C., Meckler, A. N., and Haug, G. H. (2004). Isotopic Constraints on Glacial/Interglacial Changes in the Oceanic Nitrogen Budget. *Glob. Biogeochem. Cycles* 18. doi:10.1029/2003GB002189

Domeier, M., and Torsvik, T. H. (2014). Plate Tectonics in the Late Paleozoic. *Geosci. Front.* 5, 303–350. doi:10.1016/j.gsf.2014.01.002

Doubinger, J., and Elsass, F. (1975). Nouvelles données minéralogiques et palynologiques sur les sédiments permiens du bassin d'Autun. *Bull. de la Société d'Histoire naturelle des amis du musée d'Autun* 76, 13–28.

Ducassou, C., Mercuzot, M., Bourquin, S., Rossignol, C., Pellenard, P., Beccaletto, L., et al. (2019). Sedimentology and U-Pb Dating of Carboniferous to Permian continental Series of the Northern Massif Central (France): Local Palaeogeographic Evolution and Larger Scale Correlations. *Palaeogeogr. Palaeoclimatol. Palaeoecol.* 533, 109228. doi:10.1016/j.palaeo.2019.06.001

Elsass-Damon, F. (1977). Les «schistes bitumineux» du bassin d'Autun: Pétrographie, Minéralogie, Cristallochimie, Pyrolise. Dissertation thesis. Paris (France): Université Pierre et Marie Curie.

Ertel, J. R., and Hedges, J. I. (1985). Sources of Sedimentary Humic Substances: Vascular Plant Debris. *Geochim. Cosmochim. Acta* 49, 2097–2107. doi:10.1016/0016-7037(85)90067-5

Faure, M., and Becq-Giraudon, J. F. (1993). "Sur la succession des épisodes extensifs au cours du désépaississement carbonifère du Massif central français," in *Comptes rendus de l'Académie des sciences. Série 2, Mécanique, Physique, Chimie, Sciences de l'univers, Sciences de la Terre* (Paris: Gauthier-Villars), 967–973.

Faure, M., Lardeaux, J.-M., and Ledru, P. (2009). A Review of the Pre-permian Geology of the Variscan French Massif Central. *Comptes rendus Geosci.* 341, 202–213. doi:10.1016/j.crte.2008.12.001

Faure, M. (1995). Late Orogenic Carboniferous Extensions in the Variscan French Massif Central. *Tectonics* 14, 132–153. doi:10.1029/94TC02021

Fielding, C. R., Frank, T. D., Birgenheier, L. P., Rygel, M. C., Jones, A. T., and Roberts, J. (2008). Stratigraphic Imprint of the Late Palaeozoic Ice Age in Eastern Australia: a Record of Alternating Glacial and Nonglacial Climate Regime. *J. Geol. Soc.* 165, 129–140. doi:10.1144/0016-76492007-036

Foster, G. L., Royer, D. L., and Lunt, D. J. (2017). Future Climate Forcing Potentially without Precedent in the Last 420 Million Years. *Nat. Commun.* 8, 1–8. doi:10.1038/ncomms14845

Frank, T. D., Thomas, S. G., and Fielding, C. R. (2008). On Using Carbon and Oxygen Isotope Data from Glendonites as Paleoenvironmental Proxies: a Case Study from the Permian System of Eastern Australia. *J. Sediment. Res.* 78, 713–723. doi:10.2110/jsr.2008.081

Garel, S., Behar, F., Schnyder, J., and Baudin, F. (2017). Palaeoenvironmental Control on Primary Fluids Characteristics of Lacustrine Source Rocks in the Autun Permian Basin (France). *Bull. Soc. Géol. Fr.* 188, 29. doi:10.1051/bsgf/2017187

Gastaldo, R. A., DiMichele, W. A., and Pfefferkorn, H. W. (1996). Out of the Icehouse into the Greenhouse: A Late Paleozoic Analogue for Modern Global Vegetational Change. *Gsa today* 6, 1–7.

Goddéris, Y., Donnadieu, Y., Carretier, S., Aretz, M., Dera, G., Macouin, M., et al. (2017). Onset and Ending of the Late Palaeozoic Ice Age Triggered by Tectonically Paced Rock Weathering. *Nat. Geosci.* 10, 382–386. doi:10.1038/ngeo2931

Grice, K., Nabbefeld, B., and Maslen, E. (2007). Source and Significance of Selected Polycyclic Aromatic Hydrocarbons in Sediments (Hovea-3 Well, Perth Basin, Western Australia) Spanning the Permian-Triassic Boundary. *Org. Geochem.* 38, 1795–1803. doi:10.1016/j.orggeochem.2007.07.001

Grossman, E. L., Yancey, T. E., Jones, T. E., Bruckschen, P., Chuvashov, B., Mazzullo, S. J., et al. (2008). Glaciation, Aridification, and Carbon Sequestration in the Permo-Carboniferous: The Isotopic Record from Low Latitudes. *Palaeogeogr. Palaeoclimatol. Palaeoecol.* 268, 222–233. doi:10.1016/j.palaeo.2008.03.053

Guo, H., Du, Y., Kah, L. C., Huang, J., Hu, C., Huang, H., et al. (2013). Isotopic Composition of Organic and Inorganic Carbon from the Mesoproterozoic Jixian Group, North China: Implications for Biological and Oceanic Evolution. *Precambrian Res.* 224, 169–183. doi:10.1016/j.precamres.2012.09.023

Hayes, J. M. (2001). Fractionation of Carbon and Hydrogen Isotopes in Biosynthetic Processes. *Rev. Mineral. Geochem.* 43, 225–277. doi:10.2138/gsrmg.43.1.225

Hayes, J. M. (1983). "Geochemical Evidence Bearing on the Origin of Aerobiosis, a Speculative Hypothesis," in *Earth's Earliest Biosphere: Its Origin and Evolution*. Editor J. W. Schopf (Princeton, NJ: Princeton University Press), 291–301.

Hayes, J. M., Strauss, H., and Kaufman, A. J. (1999). The Abundance of 13C in marine Organic Matter and Isotopic Fractionation in the Global Biogeochemical Cycle of Carbon during the Past 800 Ma. *Chem. Geol.* 161, 103–125. doi:10.1016/S0009-2541(99)00083-2

Hayes, J. M., Wedeking, K. W., and Kaplan, I. R. (1983). "Precambrian Organic Geochemistry-Preservation of the Record," in *Organic Geochemistry, Principles and Applications*. Editors M. H. Engel and S. A. Macko (Boston, MA: Springer), 657–684.

Herczeg, A. L., and Fairbanks, R. G. (1987). Anomalous Carbon Isotope Fractionation between Atmospheric CO2 and Dissolved Inorganic Carbon Induced by Intense Photosynthesis. *Geochim. Cosmochim. Acta* 51, 895–899. doi:10.1016/0016-7037(87)90102-5

Hoefs, J., and Frey, M. (1976). The Isotopic Composition of Carbonaceous Matter in a Metamorphic Profile from the Swiss Alps. *Geochim. Cosmochim. Acta* 40, 945–951. doi:10.1016/0016-7037(76)90143-5

Hollander, D. J., and McKenzie, J. A. (1991). CO2 Control on Carbon-Isotope Fractionation During Aqueous Photosynthesis: A Paleo-pCO2 Barometer. *Geology* 19, 929–932. doi:10.1130/0091-7613(1991)019%3C0929:CCOCIF%3E2.3.CO;2)

Hollander, D. J., McKenzie, J. A., Hsu, K. J., and Huc, A. Y. (1993). Application of an Eutrophic Lake Model to the Origin of Ancient Organic-Carbon-Rich Sediments. *Glob. Biogeochem. Cycles* 7, 157–179. doi:10.1029/92GB02831

Hyde, W. T., Crowley, T. J., Tarasov, L., and Peltier, W. R. (1999). The Pangean Ice Age: Studies with a Coupled Climate-Ice Sheet Model. *Clim. Dyn.* 15, 619–629. doi:10.1007/s003820050305

Isbell, J. L., Henry, L. C., Gulbranson, E. L., Limarino, C. O., Fraiser, M. L., Koch, Z. J., et al. (2012). Glacial Paradoxes During the Late Paleozoic Ice Age: Evaluating the Equilibrium Line Altitude as a Control on Glaciation. *Gondwana Res.* 22, 1–19. doi:10.1016/j.gr.2011.11.005

Isbell, J. L., Lenaker, P. A., Askin, R. A., Miller, M. F., and Babcock, L. E. (2003). Reevaluation of the Timing and Extent of Late Paleozoic Glaciation in Gondwana: Role of the Transantarctic Mountains. *Geol* 31, 977–980. doi:10.1130/G19810.1

Izart, A., Palhol, F., Gleixner, G., Elie, M., Blaise, T., Suarez-Ruiz, I., et al. (2012). Palaeoclimate Reconstruction from Biomarker Geochemistry and Stable Isotopes of n-Alkanes from Carboniferous and Early Permian Humic Coals and Limnic Sediments in Western and Eastern Europe. *Org. Geochem.* 43, 125–149. doi:10.1016/j.orggeochem.2011.10.004

Jenkyns, H. C. (2010). Geochemistry of Oceanic Anoxic Events. *Geochem. Geophys. Geosyst.* 11. doi:10.1029/2009GC002788

Johnston, D. T., Macdonald, F. A., Gill, B. C., Hoffman, P. F., and Schrag, D. P. (2012). Uncovering the Neoproterozoic Carbon Cycle. *Nature* 483, 320–323. doi:10.1038/nature10854

Kah, L. C., Sherman, A. G., Narbonne, G. M., Knoll, A. H., and Kaufman, A. J. (1999). δ13C Stratigraphy of the Proterozoic Bylot Supergroup, Baffin Island, Canada: Implications for Regional Lithostratigraphic Correlations. *Can. J. Earth Sci.* 36, 313–332. doi:10.1139/e98-100

Kashiyama, Y., Ogawa, N. O., Kuroda, J., Shiro, M., Nomoto, S., Tada, R., et al. (2008). Diazotrophic Cyanobacteria as the Major Photoautotrophs during Mid-cretaceous Oceanic Anoxic Events: Nitrogen and Carbon Isotopic Evidence from Sedimentary Porphyrin. *Org. Geochem.* 39, 532–549. doi:10.1016/j.orggeochem.2007.11.010

Klemme, H. D., and Ulmishek, G. F. (1991). Effective Petroleum Source Rocks of the World: Stratigraphic Distribution and Controlling Depositional Factors. *AAPG Bull.* 75, 1809–1851. doi:10.1306/0C9B2A47-1710-11D7-8645000102C1865D

Kump, L. R., and Arthur, M. A. (1999). Interpreting Carbon-Isotope Excursions: Carbonates and Organic Matter. *Chem. Geol.* 161, 181–198. doi:10.1016/S0009-2541(99)00086-8

Kuypers, M. M. M., Pancost, R. D., and Damsté, J. S. S. (1999). A Large and Abrupt Fall in Atmospheric CO2 Concentration during Cretaceous Times. *Nature* 399, 342–345. doi:10.1038/20659

Lamb, A. L., Leng, M. J., Umer Mohammed, M., and Lamb, H. F. (2004). Holocene Climate and Vegetation Change in the Main Ethiopian Rift Valley, Inferred from the Composition (C/N and δ13C) of Lacustrine Organic Matter. *Quat. Sci. Rev.* 23, 881–891. doi:10.1016/j.quascirev.2003.06.010

Lamb, A. L., Wilson, G. P., and Leng, M. J. (2006). A Review of Coastal Palaeoclimate and Relative Sea-Level Reconstructions Using δ13C and C/N Ratios in Organic Material. *Earth Sci. Rev.* 75, 29–57. doi:10.1016/j.earscirev.2005.10.003

Lehmann, M. F., Bernasconi, S. M., Barbieri, A., and McKenzie, J. A. (2002). Preservation of Organic Matter and Alteration of its Carbon and Nitrogen Isotope Composition during Simulated and *In Situ* Early Sedimentary Diagenesis. *Geochim. Cosmochim. Acta* 66, 3573–3584. doi:10.1016/S0016-7037(02)00968-7

Liu, C., Du, Y., Jarochowska, E., Yan, J., Munnecke, A., and Lu, G. (2018). A Major Anomaly in the Carbon Cycle during the Late Cisuralian (Permian): Timing, Underlying Triggers and Implications. *Palaeogeogr. Palaeoclimatol. Palaeoecol.* 491, 112–122. doi:10.1016/j.palaeo.2017.11.061

Liu, C., Jarochowska, E., Du, Y., Vachard, D., and Munnecke, A. (2017). Stratigraphical and δ13C Records of Permo-Carboniferous Platform Carbonates, South China: Responses to Late Paleozoic Icehouse Climate and Icehouse-Greenhouse Transition. *Palaeogeogr. Palaeoclimatol. Palaeoecol.* 474, 113–129. doi:10.1016/j.palaeo.2016.07.038

Malavieille, J., Guihot, P., Costa, S., Lardeaux, J. M., and Gardien, V. (1990). Collapse of the Thickened Variscan Crust in the French Massif Central: Mont Pilat Extensional Shear Zone and St. Etienne Late Carboniferous basin. *Tectonophysics* 177, 139–149. doi:10.1016/0040-1951(90)90278-G

Marteau, P. (1983). Le bassin permo-carbonifère d'Autun: stratigraphie, sédimentologie et aspects structuraux. Dissertation thesis. Dijon (France): Université de Bourgogne.

Mayer, B., and Schwark, L. (1999). A 15,000-Year Stable Isotope Record from Sediments of Lake Steisslingen, Southwest Germany. *Chem. Geol.* 161, 315–337. doi:10.1016/S0009-2541(99)00093-5

Maynard, J. R., Hofmann, W., Dunay, R. E., Benthan, P. N., Dean, K. P., and Watson, I. (1997). The Carboniferous of Western Europe; the Development of a Petroleum System. *Pet. Geosci.* 3, 97–115. doi:10.1144/petgeo.3.2.97

McArthur, A. D., Kneller, B. C., Wakefield, M. I., Souza, P. A., and Kuchle, J. (2016). Palynofacies Classification of the Depositional Elements of Confined Turbidite Systems: Examples from the Gres d'Annot, SE France. *Mar. Pet. Geol.* 77, 1254–1273. doi:10.1016/j.marpetgeo.2016.08.020

Ménard, G., and Molnar, P. (1988). Collapse of a Hercynian Tibetan Plateau into a Late Palaeozoic European Basin and Range Province. *Nature* 334, 235–237. doi:10.1038/334235a0

Mercuzot, M., Bourquin, S., Beccaletto, L., Ducassou, C., Rubi, R., and Pellenard, P. (2021). Palaeoenvironmental Reconstitutions at the Carboniferous-Permian Transition South of the Paris Basin, France: Implications on the Stratigraphic Evolution and basin Geometry. *Int. J. Earth Sci.* 110, 9–33. doi:10.1007/s00531-020-01940-7

Meyers, P. A. (2003). Applications of Organic Geochemistry to Paleolimnological Reconstructions: A Summary of Examples from the Laurentian Great Lakes. *Org. Geochem.* 34, 261–289. doi:10.1016/S0146-6380(02)00168-7

Meyers, P. A., and Ishiwatari, R. (1993). Lacustrine Organic Geochemistry-An Overview of Indicators of Organic Matter Sources and Diagenesis in lake Sediments. *Org. Geochem.* 20, 867–900. doi:10.1016/0146-6380(93)90100-P

Meyers, P. A., and Ishiwatari, R. (1995). "Organic Matter Accumulation Records in Lake Sediments," in *Physics and Chemistry of Lakes*. Editors A. Lerman, D. Imboden, and J. Gat (Berlin, Germany: Springer), 279–328.

Meyers, P. A. (1994). Preservation of Elemental and Isotopic Source Identification of Sedimentary Organic Matter. *Chem. Geol.* 114, 289–302. doi:10.1016/0009-2541(94)90059-0

Meyers, P. A., and Teranes, J. L. (2001). "Sediment Organic Matter," in *Tracking Environmental Change Using Lake Sediments 2: Physical and Geochemical Methods*. Editors W. M. Last and J. P. Smol (Dordrecht, Netherlands: Kluwer Academic Publishers), 239–269.

Meyers, P. A. (2014). Why are the δ13Corgvalues in Phanerozoic Black Shales More Negative Than in Modern marine Organic Matter?. *Geochem. Geophys. Geosyst.* 15, 3085–3106. doi:10.1002/2014GC005305

Mii, H.-S., Grossman, E. L., Yancey, T. E., Chuvashov, B., and Egorov, A. (2001). Isotopic Records of Brachiopod Shells from the Russian Platform - Evidence for the Onset of Mid-carboniferous Glaciation. *Chem. Geol.* 175, 133–147. doi:10.1016/S0009-2541(00)00366-1

Mii, H. S., Grossman, E. L., and Yancey, T. E. (1999). Carboniferous Isotope Stratigraphies of North America: Implications for Carboniferous Paleoceanography and Mississippian Glaciation. *Geol. Soc. Am. Bull.* 111, 960–973. doi:10.1130/0016-7606(1999)111<0960:CISONA>2.3.CO;2

Monin, J. C., Boudou, J. P., Durand, B., and Oudin, J. L. (1981). Example of the Enrichment of Carbon-13 in Coals in the Process of Coalification. *Fuel* 60, 957–960. doi:10.1016/0016-2361(81)90091-0

Montañez, I. P. (2016). A Late Paleozoic Climate Window of Opportunity. *Proc. Natl. Acad. Sci. USA* 113, 2334–2336. doi:10.1073/pnas.1600236113

Montañez, I. P., and Poulsen, C. J. (2013). The Late Paleozoic Ice Age: an Evolving Paradigm. *Annu. Rev. Earth Planet. Sci.* 41, 629–656. doi:10.1146/annurev.earth.031208.100118

Montañez, I. P., Tabor, N. J., Niemeier, D., DiMichele, W. A., Frank, T. D., Fielding, C. R., et al. (2007). CO2-forced Climate and Vegetation Instability during Late Paleozoic Deglaciation. *Science* 315, 87–91. doi:10.1126/science.1134207

Müller, A. B., Strauss, H., Hartkopf-Fröder, C., and Littke, R. (2006). Reconstructing the Evolution of the Latest Pennsylvanian-Earliest Permian Lake Odernheim Based on Stable Isotope Geochemistry and Palynofacies: A Case Study from the Saar-Nahe Basin, Germany. *Palaeogeogr. Palaeoclimatol. Palaeoecol.* 240, 204–224. doi:10.1016/j.palaeo.2006.03.049

Nordt, L., Tubbs, J., and Dworkin, S. (2016). Stable Carbon Isotope Record of Terrestrial Organic Materials for the Last 450 Ma yr. *Earth Sci. Rev.* 159, 103–117. doi:10.1016/j.earscirev.2016.05.007

Opdyke, N. D., Mushayandebvu, M., and De Wit, M. J. (2001). A New Palæomagnetic Pole for the Dwyka System and Correlative Sediments in Sub-saharan Africa. *J. Afr. Earth Sci.* 33, 143–153. doi:10.1016/S0899-5362(01)90095-8

Pellenard, P., Gand, G., Schmitz, M., Galtier, J., Broutin, J., and Stéyer, J.-S. (2017). High-precision U-Pb Zircon Ages for Explosive Volcanism Calibrating the NW European Continental Autunian Stratotype. *Gondwana Res.* 51, 118–136. doi:10.1016/j.gr.2017.07.014

Peters, K. E., Sweeney, R. E., and Kaplan, I. R. (1978). Correlation of Carbon and Nitrogen Stable Isotope Ratios in Sedimentary Organic Matter 1. *Limnol. Oceanogr.* 23, 598–604. doi:10.4319/lo.1978.23.4.0598

Peters-Kottig, W., Strauss, H., and Kerp, H. (2006). The Land Plant δ13C Record and Plant Evolution in the Late Palaeozoic. *Palaeogeogr. Palaeoclimatol. Palaeoecol.* 240, 237–252. doi:10.1016/j.palaeo.2006.03.051

Powell, C. M., and Veevers, J. J. (1987). Namurian Uplift in Australia and South America Triggered the Main Gondwanan Glaciation. *Nature* 326, 177–179. doi:10.1038/326177a0

Prokopenko, M. G., Hammond, D. E., and Stott, L. (2006). Lack of Isotopic Fractionation of δ15N of Organic Matter During Long-Term Diagenesis in marine Sediments, ODP Leg 202, Sites 1234 and 1235. *Proc. Ocean Drill. Program Sci. Results* 202..

Ramaswamy, V., Gaye, B., Shirodkar, P. V., Rao, P. S., Chivas, A. R., Wheeler, D., et al. (2008). Distribution and Sources of Organic Carbon, Nitrogen and Their Isotopic Signatures in Sediments from the Ayeyarwady (Irrawaddy) continental Shelf, Northern Andaman Sea. *Mar. Chem.* 111, 137–150. doi:10.1016/j.marchem.2008.04.006

Retallack, G. J. (2013). Permian and Triassic Greenhouse Crises. *Gondwana Res.* 24, 90–103. doi:10.1016/j.gr.2012.03.003

Retallack, G. J., Sheldon, N. D., Carr, P. F., Fanning, M., Thompson, C. A., Williams, M. L., et al. (2011). Multiple Early Triassic Greenhouse Crises Impeded Recovery from Late Permian Mass extinctionHydrogen Isotope Ratios of Recent Lacustrine Sedimentary n-Alkanes Record Modern Climate Variability. *Palaeogeogr. Palaeoclimatol. Palaeoecol.* 308, 233–251. doi:10.1016/j.palaeo.2010.09.022

Roscher, M., and Schneider, J. W. (2006). Permo-Carboniferous Climate: Early Pennsylvanian to Late Permian Climate Development of Central Europe in a Regional and Global Context. *Geol. Soc. Spec. Publ.* 265, 95–136. doi:10.1144/GSL.SP.2006.265.01.05

Sachse, D., Radke, J., and Gleixner, G. (2004). Hydrogen Isotope Ratios of Recent Lacustrine Sedimentary n-1137 Alkanes Record Modern Climate Variability. *Geochim. Cosmochim. Acta* 68, 4877–4889. doi:10.1016/j.gca.2004.06.004

Sage, R. F. (2004). The Evolution of C4photosynthesis. *New Phytol.* 161, 341–370. doi:10.1111/j.1469-8137.2004.00974.x

Saltzman, M., Groessens, E., and Zhuravlev, A. (2004). Carbon Cycle Models Based on Extreme Changes in δ13C: An Example from the Lower Mississippian. *Palaeogeogr. Palaeoclimatol. Palaeoecol.* 213, 359–377. doi:10.1016/j.palaeo.2004.07.01910.1016/s0031-0182(04)00389-x

Saltzman, M. R. (2005). Phosphorus, Nitrogen, and the Redox Evolution of the Paleozoic Oceans. *Geology* 33, 573–576. doi:10.1130/G21535.1

Schidlowski, M., Hayes, J. M., and Kaplan, I. R. (1983). "Isotopic Inferences of Ancient Biochemistries-Carbon, Sulfur, Hydrogen, and Nitrogen," in *Earth's Earliest Biosphere: Its Origin and Evolution*. Editors J. W. Schopf (Princeton, NJ: Princeton University Press), 149–186.

Schnyder, J., Dejax, J., Keppens, E., Nguyen Tu, T. T., Spagna, P., Boulila, S., et al. (2009). An Early Cretaceous Lacustrine Record: Organic Matter and Organic Carbon Isotopes at Bernissart (Mons Basin, Belgium). *Palaeogeogr. Palaeoclimatol. Palaeoecol.* 281, 79–91. doi:10.1016/j.palaeo.2009.07.014

Schnyder, J., Martinez, M., Baudin, F., Mercuzot, M., Pellenard, P., Thomazo, C., et al. (2020). *Long-Term Lacustrine Paleo-Productivity And/or Paleo-Anoxia Trends Controlled by Eccentricity Cycles in the continental Autun Basin (France) at the Carboniferous/Permian Boundary*, Vienna.

Schnyder, J., Stetten, E., Baudin, F., Pruski, A. M., and Martinez, P. (2017). Palynofacies Reveal Fresh Terrestrial Organic Matter Inputs in the Terminal Lobes of the Congo Deep-Sea Fan. *Deep Sea Res. Part Top. Stud. Oceanogr.* 142, 91–108. doi:10.1016/j.dsr2.2017.05.008

Schubert, C. J., and Calvert, S. E. (2001). Nitrogen and Carbon Isotopic Composition of marine and Terrestrial Organic Matter in Arctic Ocean Sediments:. *Deep Sea Res. Oceanographic Res. Pap.* 48, 789–810. doi:10.1016/S0967-0637(00)00069-8

Schwarzbauer, J., and Jovančićević, B. (2015). *Fundamentals in Organic Geochemistry – Fossil Matter in the Geosphere.* Cham, CH: Springer.

Scotese, C. R. (2016). PALEOMAP PaleoAtlas for GPlates and the PaleoData Plotter Program, PALEOMAP Project. Available at: http://www.earthbyte.org/paleomap-paleoatlas-for-gplates (Accessed June 17, 2021).

Sephton, M. A., Amor, K., Franchi, I. A., Wignall, P. B., Newton, R., and Zonneveld, J. P. (2002). Carbon and Nitrogen Isotope Disturbances and an End-Norian (Late Triassic) Extinction Event. *Geology* 30, 1119–1122. doi:10.1130/0091-7613(2002)030%3C1119:CANIDA%3E2.0.CO;2

Sigman, D. M., Karsh, K. L., and Casciotti, K. L. (2009). "Ocean Process Tracers: Nitrogen Isotopes in the Ocean," in *Encyclopedia of Ocean Sciences.* Editor J. H. Steele (London, Elsevier Ltd), 40–54.

Soreghan, G. S., Soreghan, M. J., and Heavens, N. G. (2019). Explosive Volcanism as a Key Driver of the Late Paleozoic Ice Age. *Geology* 47, 600–604. doi:10.1130/G46349.1

Steffen, D., and Gorin, G. E. (1993). "Sedimentology of Organic Matter in Upper Tithonian-Berriasian Deep-Sea Carbonates of Southeast France: Evidence of Eustatic Control," in *Source Rocks in a Sequence Stratigraphic Framework.* Editors B. J. Katz and L. M. Pratt (Tulsa, OK: AAPG Studies on Geology), 49–65.

Stollhofen, H., Frommherz, B., and Stanistreet, I. G. (1999). Volcanic Rocks as Discriminants in Evaluating Tectonic versus Climatic Control on Depositional Sequences, Permo-Carboniferous continental Saar-Nahe Basin. *J. Geol. Soc.* 156, 801–808. doi:10.1144/gsjgs.156.4.0801

Strauss, H., Des Marais, D. J., Hayes, J. M., and Summons, R. E. (1992). "Proterozoic Organic Carbon—Its Preservation and Isotopic Record," in *Early Organic Evolution.* Editor M. Schidlowski, S. Golubic, M. M. Kimberley, D. M. McKirdy, and P. A. Trudinger (Berlin: Springer), 203–211. doi:10.1007/978-3-642-76884-2_14

Strauss, H., and Peters-Kottig, W. (2003). The Paleozoic to Mesozoic Carbon Cycle Revisited: The Carbon Isotopic Composition of Terrestrial Organic Matter. *Geochem. Geophys. Geosyst.* 4, 1083. doi:10.1029/2003GC000555

Thomasson, J. R., Nelson, M. E., and Zakrzewski, R. J. (1986). A Fossil Grass (Gramineae: Chloridoideae) from the Miocene with Kranz Anatomy. *Science* 233, 876–878. doi:10.1126/science.233.4766.876

Thomazo, C., Pinti, D. L., Busigny, V., Ader, M., Hashizume, K., and Philippot, P. (2009). Biological Activity and the Earth's Surface Evolution: Insights from Carbon, Sulfur, Nitrogen and Iron Stable Isotopes in the Rock Record. *Comptes Rendus Palevol* 8, 665–678. doi:10.1016/j.crpv.2009.02.003

Tocqué, E., Behar, F., Budzinski, H., and Lorant, F. (2005). Carbon Isotopic Balance of Kerogen Pyrolysis Effluents in a Closed System. *Org. Geochem.* 36, 893–905. doi:10.1016/j.orggeochem.2005.01.007

Tramoy, R., Salpin, M., Schnyder, J., Person, A., Sebilo, M., Yans, J., et al. (2016b). Stepwise Palaeoclimate Change across the Eocene–Oligocene Transition Recorded in continental NW Europe by Mineralogical Assemblages and $\delta^{15}N_{org}$ (Rennes Basin, France). *Terra Nova* 28, 212–220. doi:10.1111/ter.12212

Tramoy, R., Schnyder, J., Nguyen Tu, T. T., Yans, J., Jacob, J., Sebilo, M., et al. (2016a). The Pliensbachian-Toarcian Paleoclimate Transition: New Insights

from Organic Geochemistry and C, H, N Isotopes in a continental Section from Central Asia. *Palaeogeogr. Palaeoclimatol. Palaeoecol.* 461, 310–327. doi:10.1016/j.palaeo.2016.08.020

Trümper, S., Germann, S., Schneider, J. W., Mertmann, D., Götze, J., and Rößler, R. (2020). Petrified Trees of the Kyffhäuser (Pennsylvanian, Thuringia): Growth Habitat, Fossilisation and Palaeoclimatic-Palaeoecological Implications. *Zeitschrift der Dtsch. Gesellschaft fur Geowissenschaften.* 171, 277–321. doi:10.1127/zdgg/2020/0238

Tyson, R. V. (1995). Palynological Kerogen Classification. *Sediment. Org. Matter* 341–365. doi:10.1007/978-94-011-0739-6_20

Valle, B., Courel, L., and Gelard, J. P. (1988). Les Marqueurs de la tectonique synsedimentaire et syndiagenetique dans le bassin stephanien a regime cisaillant de Blanzy-Montceau (Massif Central, France). *Bull. Soc. Géol. Fr.* 4, 529–540. doi:10.2113/gssgfbull.iv.4.529

Van Den Driessche, J., and Brun, J.-P. (1992). Tectonic Evolution of the Montagne Noire (French Massif Central): A Model of Extensional Gneiss Dome. *Geodinamica Acta* 5, 85–97. doi:10.1080/09853111.1992.11105221

Van Den Driessche, J., and Brun, J. P. (1989). "Un modèle cinématique de l'extension paléozoïque supérieur dans le Sud du Massif Central," in *Comptes rendus de l'Académie des sciences. Série 2, Mécanique, Physique, Chimie, Sciences de l'univers, Sciences de la Terre.* 1607–1613.

Van Mooy, B. A. S., Keil, R. G., and Devol, A. H. (2002). Impact of Suboxia on Sinking Particulate Organic Carbon: Enhanced Carbon Flux and Preferential Degradation of Amino Acids via Denitrification. *Geochim. Cosmochim. Acta* 66, 457–465. doi:10.1016/S0016-7037(01)00787-6

Veevers, J. J. (1994). "Pangea: Evolution of a Supercontinent and its Consequences for Earth's Paleoclimate and Sedimentary Environments," in *Pangea: Paleoclimate, Tectonics, and Sedimentation during Accretion, Zenith, and Breakup of a Supercontinent.* Editor G. O. Klein (Boulder, CO: Geological Society of America Special Paper 288), 13–24.

Wang, W., Guan, C., Zhou, C., Peng, Y., Pratt, L. M., Chen, X., et al. (2017). Integrated Carbon, Sulfur, and Nitrogen Isotope Chemostratigraphy of the Ediacaran Lantian Formation in South China: Spatial Gradient, Ocean Redox Oscillation, and Fossil Distribution. *Geobiology* 15, 552–571. doi:10.1111/gbi.12226

Yans, J., Gerards, T., Gerrienne, P., Spagna, P., Dejax, J., Schnyder, J., et al. (2010). Carbon-Isotope Analysis of Fossil wood and Dispersed Organic Matter from the Terrestrial Wealden Facies of Hautrage (Mons Basin, Belgium). *Palaeogeogr. Palaeoclimatol. Palaeoecol.* 291, 85–105. doi:10.1016/j.palaeo.2010.01.014